CSPAR-UAH

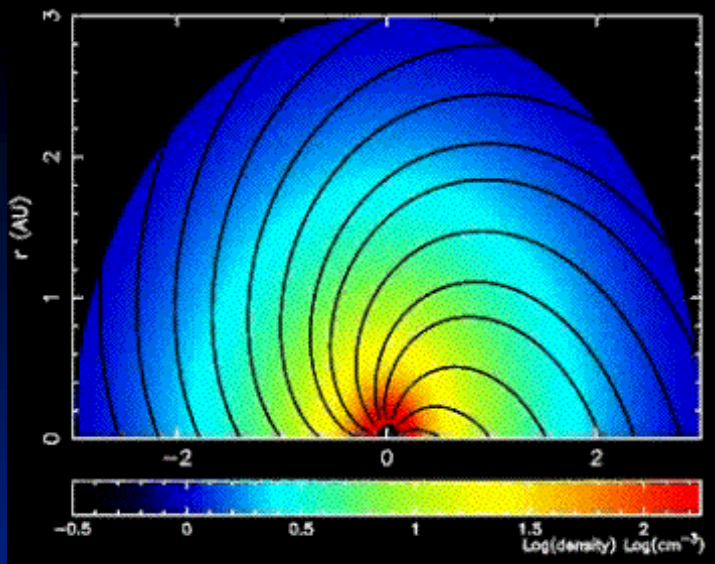

Review of Diffusive Shock Acceleration Modeling of Solar Energetic Particle Events

G.P. Zank

Gang Li, Olga Verkhoglyadova, Junxiang Hu

Center for Space and Aeronomic Research (CSPAR)

Department of Space Science

University of Alabama in Huntsville

CSPAR-UAH

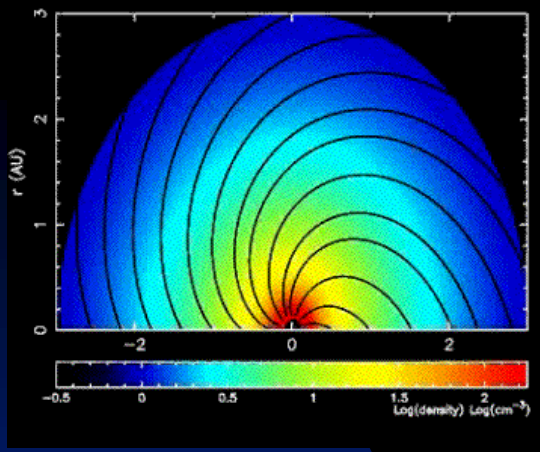

Particle Acceleration at Interplanetary Shocks

Review particle acceleration by interplanetary shocks:

1. *Interplanetary shock acceleration is fundamentally time-dependent*
2. *Interplanetary shock acceleration is fundamentally multi-dimensional spatially*
3. *Insights and extensions from basic steady-state 1D models*
4. *Unsteady diffusive shock acceleration at a quasi-parallel and quasi-perpendicular shocks for protons and heavy ions*
5. *New 2D model: iPATH*

Physics Reports 557 (2015) 1–23

Contents lists available at ScienceDirect

Physics Reports

journal homepage: www.elsevier.com/locate/physrep

A theoretical perspective on particle acceleration by interplanetary shocks and the Solar Energetic Particle problem

Olga P. Verkhoglyadova [a,b,*], Gary P. Zank [c,a], Gang Li [c,a]

Further details related to the 1D time-dependent modeling can found here.

Two Classes of Solar Energetic Particle Events

CME-Associated (Gradual Event)

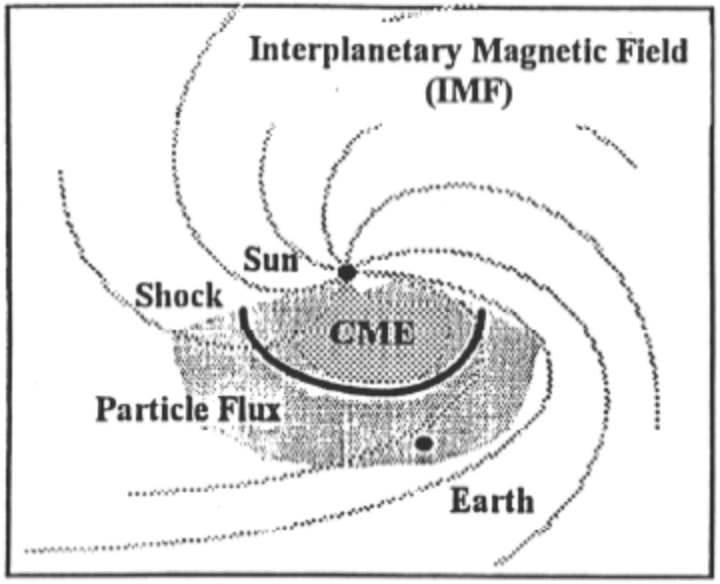

Proton-Rich
Long-Lived (Days)
60-180 Degrees Solar Longitude

$Fe/O \approx 0.1 - 0.2$
$^3He/^4He \approx .0004$
$Q(Fe) \approx 14$
Shocks accelerate solar wind

Impulsive Flare-Associated (Impulsive Event)

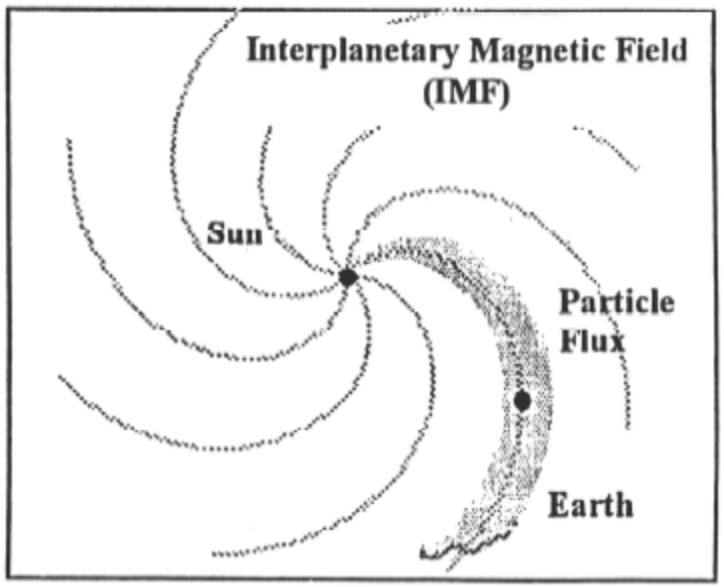

Electron-Rich
Short-Lived (Hours)
30-45 Degrees Solar Longitude

$Fe/O \approx 1$
$^3He/^4He \approx 0.1 - 10$
$Q(Fe) \approx 20$
Heated flare material accelerated

Criteria summarized by Reames (1995)

Basic diffusive shock acceleration theory

Parallel shock

shock

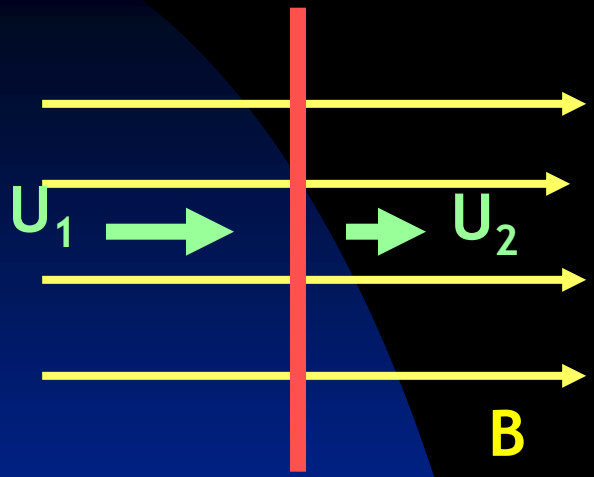

- *Acceleration time can be very long.*
- *Can accelerate thermal-energy particles - often regarded as good "injectors"*

Perpendicular shock

shock

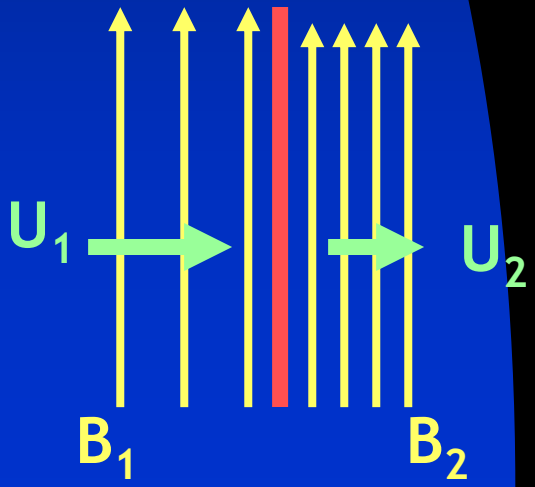

- *Acceleration time is very short compared to a parallel shock*
- *Cannot easily accelerate low energy particles - often regarded as poor "injectors"*

Diffusive shock acceleration

- The accelerated particle intensities are constant downstream of the shock and exponentially decaying upstream of the shock.
- The scale length of the decay is determined by the momentum dependent diffusion coefficient (steady state solution).

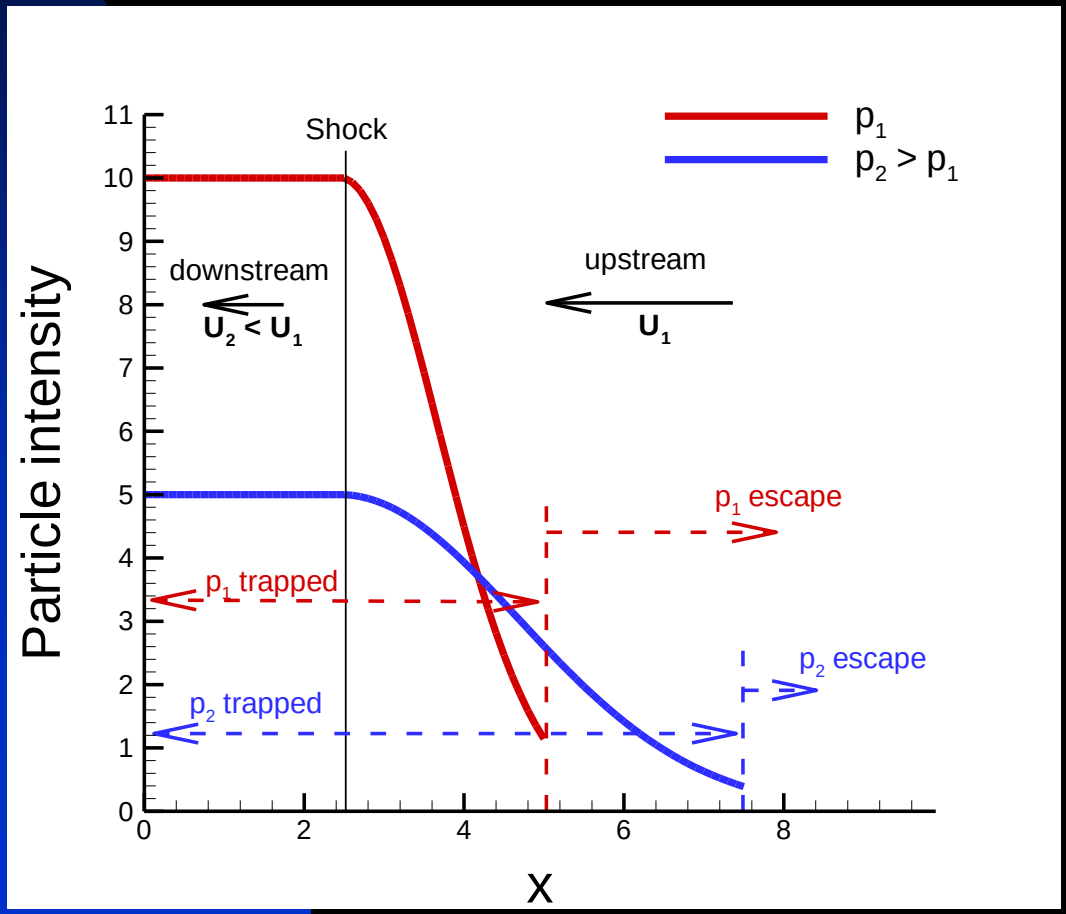

Trapped particles

- convect
- cool
- diffuse.

Escaped particles

- Transport to 1 AU (weak scattering).

Shock geometry

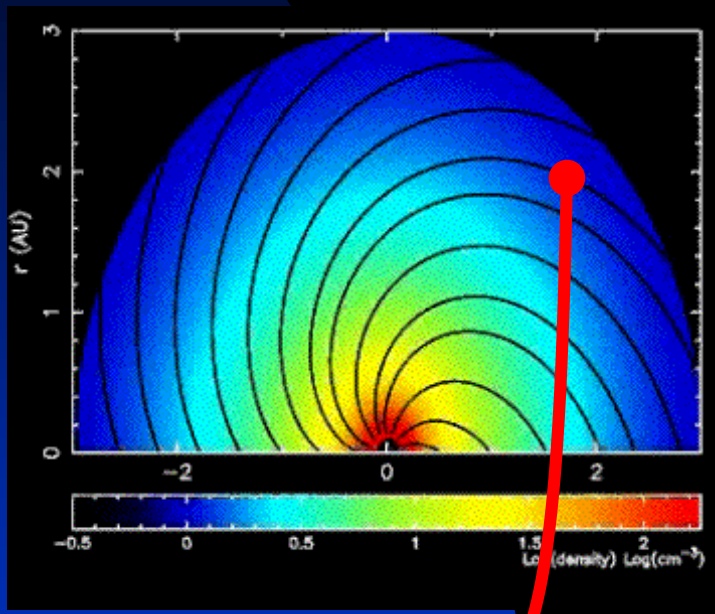

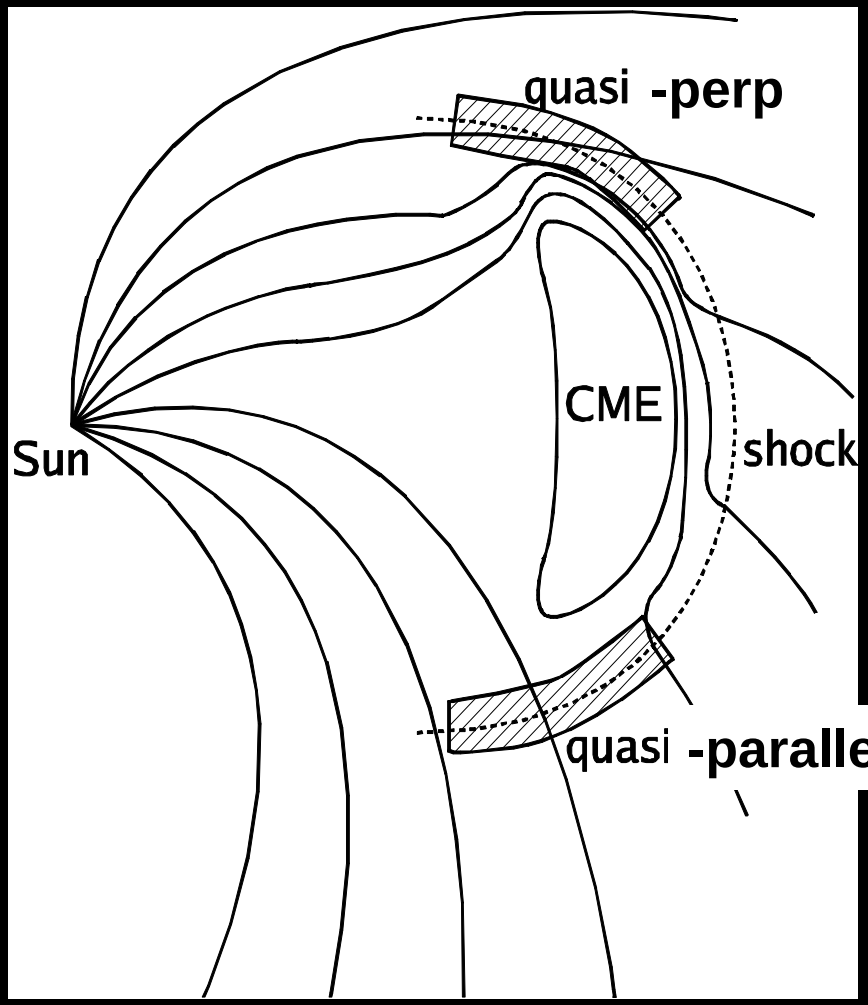

Red dot (spacecraft) connected to quasi-perpendicular shock initially and the connection gradually evolves to much more quasi-parallel configuration.

$$\tau_{convect} \sim L/U$$

$$\tau_{DYN} \sim R/(dR/dt) \quad \Rightarrow \tau_{\theta} \sim \sqrt{\frac{L}{U} R/(dR/dt)}$$

Shock geometry

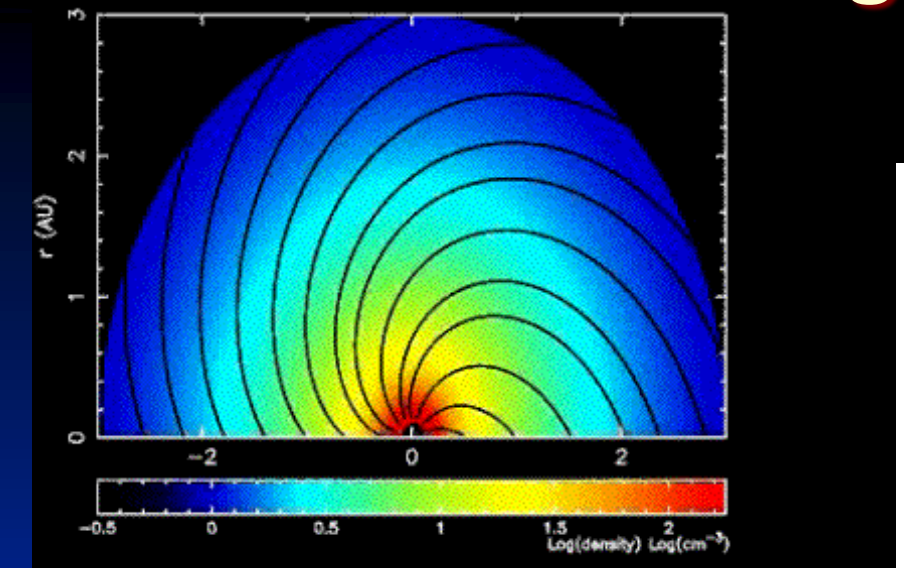

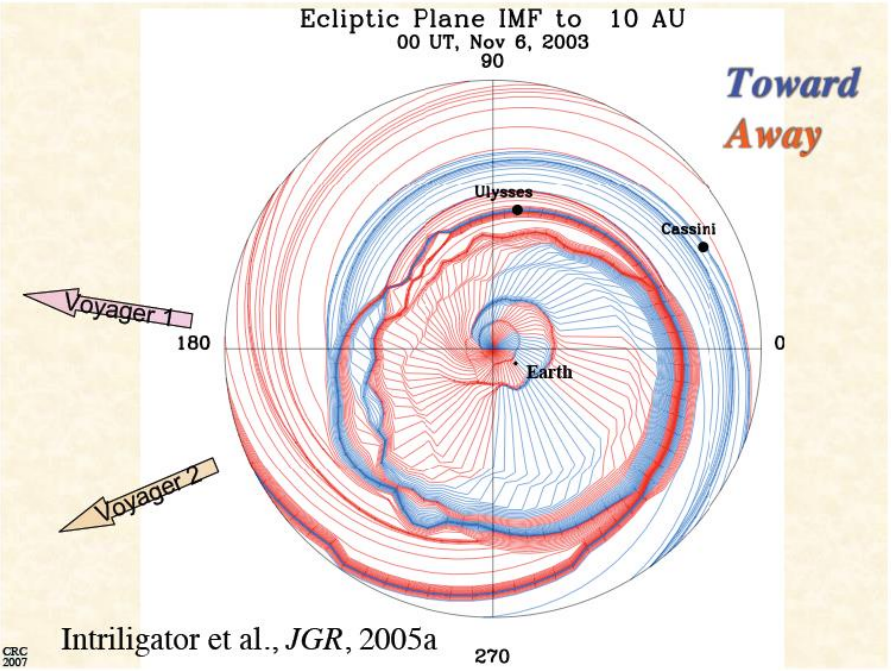

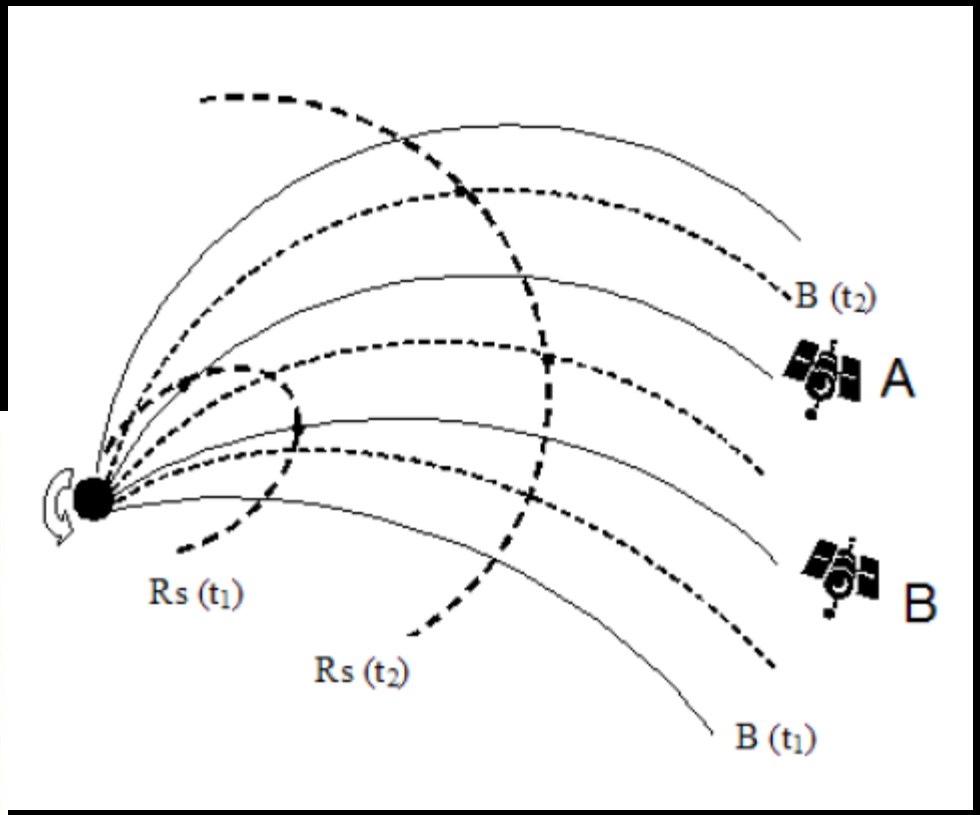

Time scales for the SEP/ESP problem

- Shock propagation in an inhomogeneous solar wind – expanding, decelerating, decreasing magnetic field strength, in situ turbulence convection, decay, driving, variability of shock normal
- Particle acceleration time scales; maximum energy, shock obliquity
- Variability in generation of shock turbulence by streaming energetic particles; particle trapping and escape
- Diffusive time scales (diffusive mfp)
- Transport time scales/length scales (transport mfp)

The shock itself introduces a multiplicity of time scales, ranging from shock propagation time scales to particle acceleration time scales at parallel and perpendicular shocks, and many of these time scales feed into other time scales (such as determining maximum particle energy scalings, escape time scales, etc.).

Shock position, velocity and compression ratio are computed from 0.1 AU to up to several AU.

Simulation results of the shock velocity dependence on radial distance from the Sun. The decaying shock propagates from 0.1 AU, reaching a compression ratio of about 1.8 at 1AU. The modeling was performed for 61 shells.

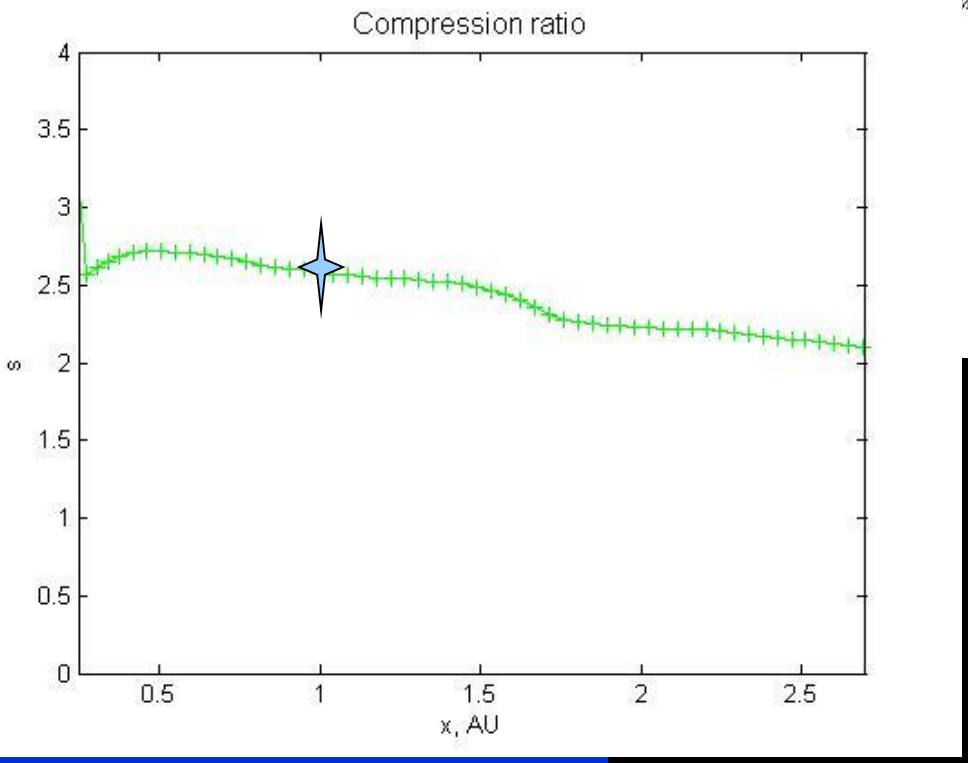

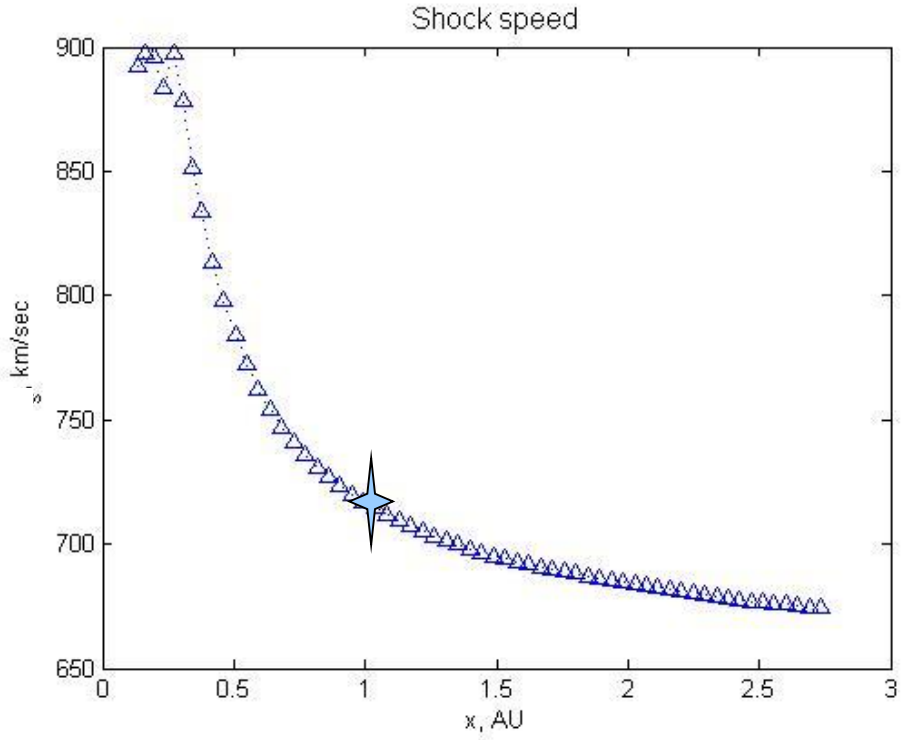

SEP Event # 215 (shock arrival at ACE: Sept. 29, 2001, 09:06 UT)

- Shock dynamical time scale:
- Post-shock complex time scales: Convection, adiabatic expansion

$$\tau_{DYNAMICAL} = \frac{R(t)}{dR/dt}$$

- Magnetic field change:

$$\frac{B}{B_0} = \left(\frac{R_0}{r}\right)^2 \left[1 + \left(\frac{W_0 R_0}{u}\right)^2 \left(\frac{r}{R_0} - 1\right)^2 \sin^2 q\right]^{1/2}$$

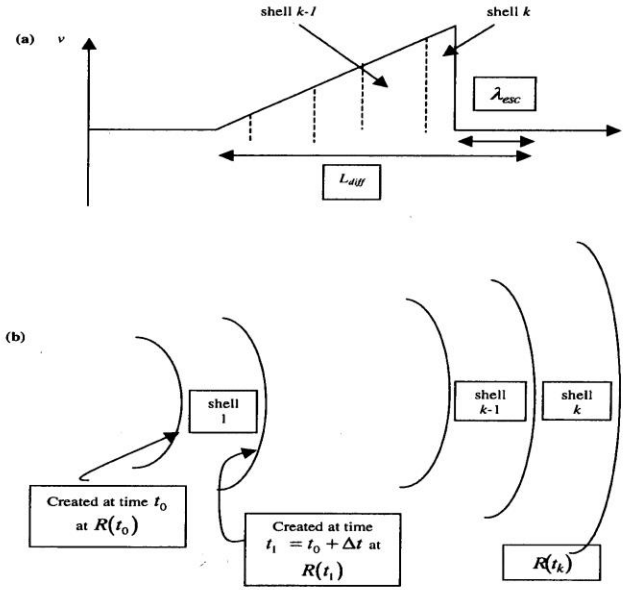

Figure 1. (a) Schematic of the density structure of an interplanetary blast wave. The total structure is subdivided into a series of concentric shells with the most recently formed shells labeled k-1 and k. Two length scales are identified: the escape length scale ahead of the shock front, λ_{esc}, beyond which energetic particles do not scatter diffusively back to the shock, and the scale size of the structure within which energetic ions are transported diffusively, L_{diff}. (b) A related schematic showing the concentric shells and their formation time as the shock propagates into the inhomogeneous solar wind. At time t_k the shock front is located at $R(t_k)$, which creates the edge of the outermost shell, identified as shell k. After formation the shells continue to evolve, being convected with the solar wind and expanding adiabatically.

JGR, Zank et. al. Vol. 105 p 25,079-25,095

Example:
Sedov-Taylor blast wave

$$R(t) = \left(E/\rho\right)^{1/5} t^{2/5}$$

$$\Rightarrow R/dR/dt = \frac{2}{5}t$$

- Post-shock complex time scales: Convection, adiabatic expansion, growth of post shock region and weakening of shock front.

$$\delta v(t) = \frac{\delta v_i}{\sqrt{1+(\alpha_v \delta v_i)t}} \qquad \alpha_v \equiv \frac{C_{f0}^2 + \gamma C_{sd0}^2 + 2C_{A0}^2}{2C_{f0}^2}$$

$$t = t_i$$

$$t = t_{i+1} = t_i + \Delta t$$

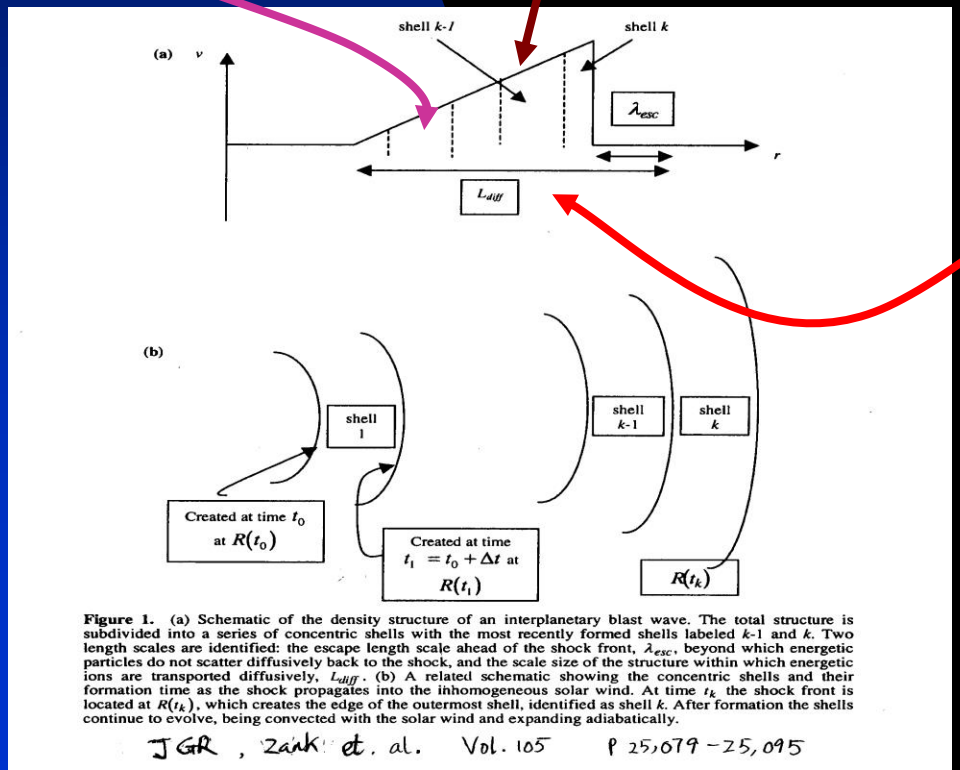

Figure 1. (a) Schematic of the density structure of an interplanetary blast wave. The total structure is subdivided into a series of concentric shells with the most recently formed shells labeled k-1 and k. Two length scales are identified: the escape length scale ahead of the shock front, λ_{esc}, beyond which energetic particles do not scatter diffusively back to the shock, and the scale size of the structure within which energetic ions are transported diffusively, L_{diff}. (b) A related schematic showing the concentric shells and their formation time as the shock propagates into the inhomogeneous solar wind. At time t_k the shock front is located at $R(t_k)$, which creates the edge of the outermost shell, identified as shell k. After formation the shells continue to evolve, being convected with the solar wind and expanding adiabatically.

JGR, Zank et. al. Vol. 105 P 25,079-25,095

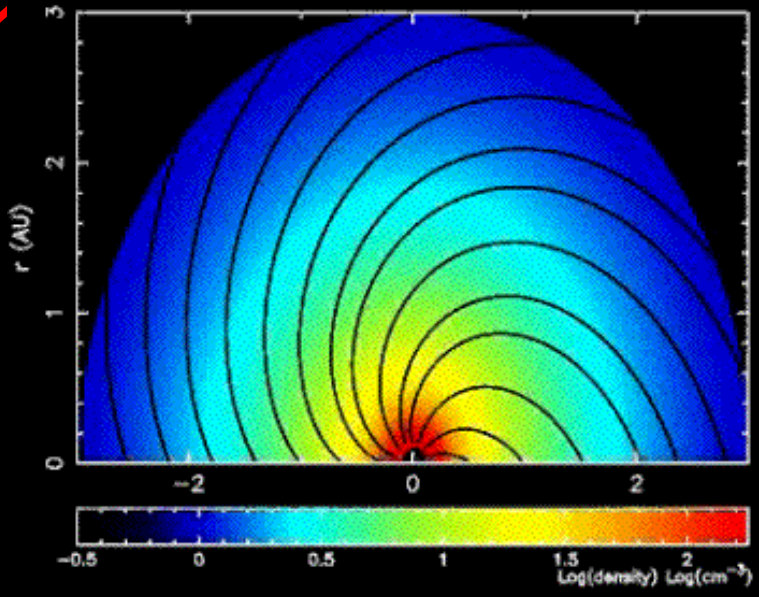

$$\frac{\partial f}{\partial t} = -U_i \frac{\partial f}{\partial x_i} + \nabla\cdot U \frac{p}{3}\frac{\partial f}{\partial p} + \nabla\cdot\left(K\cdot\nabla f\right) + Q$$

convection energy change diffusion source

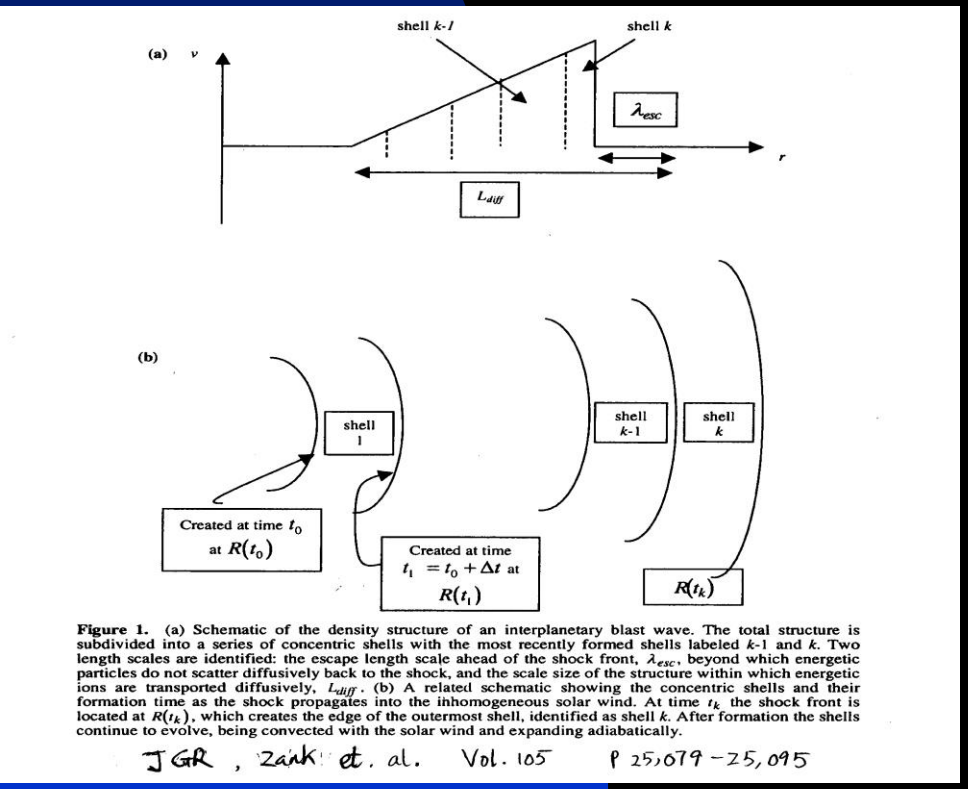

Figure 1. (a) Schematic of the density structure of an interplanetary blast wave. The total structure is subdivided into a series of concentric shells with the most recently formed shells labeled k-1 and k. Two length scales are identified: the escape length scale ahead of the shock front, λ_{esc}, beyond which energetic particles do not scatter diffusively back to the shock, and the scale size of the structure within which energetic ions are transported diffusively, L_{diff}. (b) A related schematic showing the concentric shells and their formation time as the shock propagates into the inhomogeneous solar wind. At time t_k the shock front is located at $R(t_k)$, which creates the edge of the outermost shell, identified as shell k. After formation the shells continue to evolve, being convected with the solar wind and expanding adiabatically.

JGR, Zank et. al. Vol. 105 p 25,079-25,095

$$\frac{\partial f}{\partial t} + U\frac{\partial f}{\partial r} = 0$$

$$f_i(t_k) = f_i\left[r_i(t_k) - \int_{t_{k-1}}^{t_k} U\left(r_i(t)\right)dt\right]$$

$$\frac{\partial f}{\partial t} = -U_i \frac{\partial f}{\partial x_i} + \nabla \cdot U \frac{p}{3} \frac{\partial f}{\partial p} + \nabla \cdot \left(K \cdot \nabla f \right) + Q$$

convection | energy change | diffusion | source

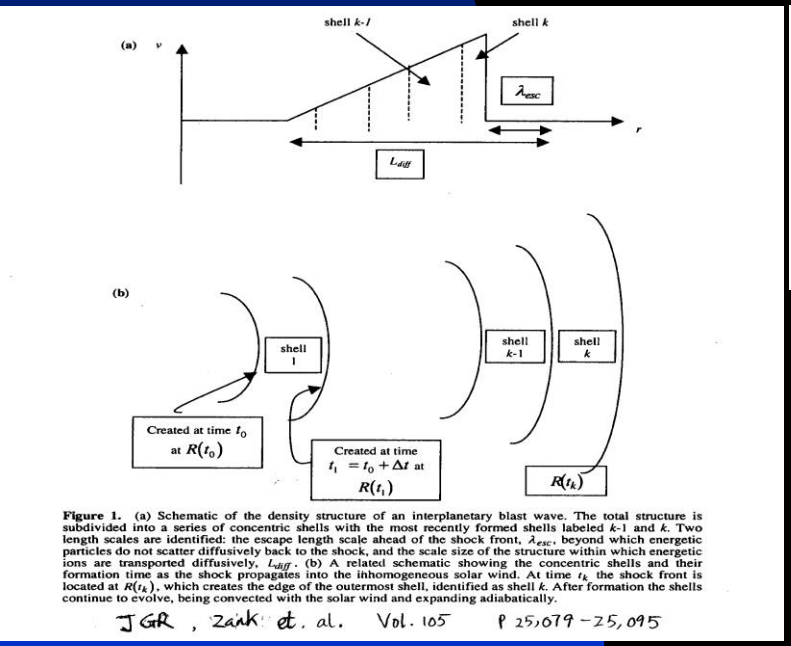

Figure 1. (a) Schematic of the density structure of an interplanetary blast wave. The total structure is subdivided into a series of concentric shells with the most recently formed shells labeled k-1 and k. Two length scales are identified: the escape length scale ahead of the shock front, λ_{esc}, beyond which energetic particles do not scatter diffusively back to the shock, and the scale size of the structure within which energetic ions are transported diffusively, L_{diff}. (b) A related schematic showing the concentric shells and their formation time as the shock propagates into the inhomogeneous solar wind. At time t_k the shock front is located at $R(t_k)$, which creates the edge of the outermost shell, identified as shell k. After formation the shells continue to evolve, being convected with the solar wind and expanding adiabatically.

JGR, Zank et. al. Vol. 105 p 25,079-25,095

$$\frac{\partial f}{\partial t} = \nabla \cdot U \frac{p}{3} \frac{\partial f}{\partial p}$$

$$\ln p\left(t_k\right) = \ln p\left(t_{k-1}\right) - \frac{1}{3} \int_{t_{k-1}}^{t_k} \frac{U}{r} dt - \ln\left[U\left(t_k\right) / U\left(t_{k-1}\right) \right]^{1/3}$$

$$\frac{\partial f}{\partial t} = -U_i \frac{\partial f}{\partial x_i} + \nabla\cdot U \frac{p}{3}\frac{\partial f}{\partial p} + \nabla\cdot\left(K\cdot\nabla f\right) + Q$$

convection energy change diffusion source

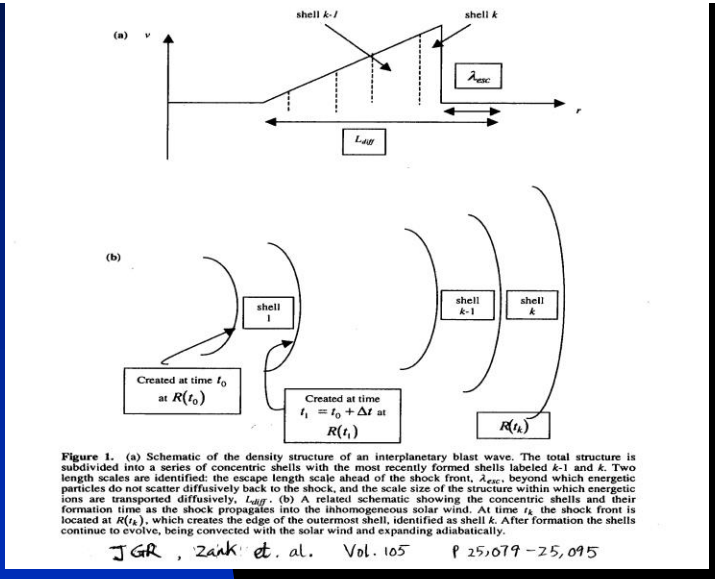

Figure 1. (a) Schematic of the density structure of an interplanetary blast wave. The total structure is subdivided into a series of concentric shells with the most recently formed shells labeled k-1 and k. Two length scales are identified: the escape length scale ahead of the shock front, λ_{esc}, beyond which energetic particles do not scatter diffusively back to the shock, and the scale size of the structure within which energetic ions are transported diffusively, L_{diff}. (b) A related schematic showing the concentric shells and their formation time as the shock propagates into the inhomogeneous solar wind. At time t_k the shock front is located at $R(t_k)$, which creates the edge of the outermost shell, identified as shell k. After formation the shells continue to evolve, being convected with the solar wind and expanding adiabatically.

JGR, Zank et. al. Vol. 105 p 25,079-25,095

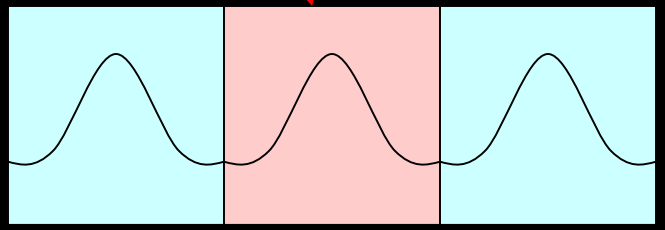

$$\frac{\partial f}{\partial t} = \frac{1}{r^2}\frac{\partial}{\partial r}\left(r^2\kappa\frac{\partial f}{\partial r}\right)$$

$$f_i\left(t_k, p, r\right) = \frac{1}{\sqrt{\pi}}\frac{f_i^{\,n}\left(t_{k-1}, p\right)}{4\pi r_i^2\left(t_k\right)}\frac{1}{\sqrt{4\kappa\left(t_k - t_{k-1}\right) + \left(\kappa/U_1\right)^2}}\exp\left[\frac{\left(r - r_i\left(t_k\right)\right)^2}{4\kappa\left(t_k - t_{k-1}\right) + \left(\kappa/U_1\right)^2}\right]$$

Particle acceleration time scales

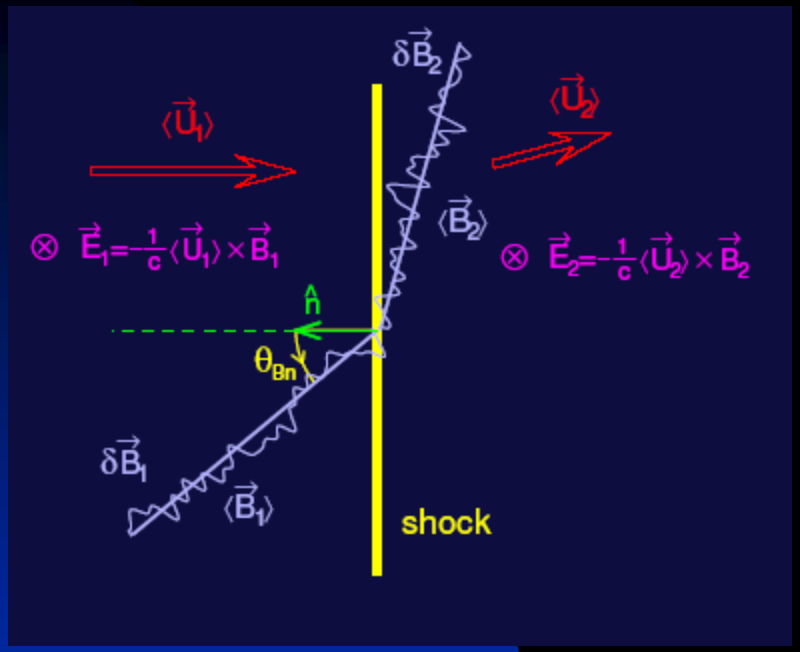

$$\frac{\Delta p}{p} = \frac{U_1 - U_2}{3}\frac{\Delta t}{L}$$

$$L = \kappa / U_1$$

$$\Rightarrow \Delta t = \frac{3U_1}{U_1 - U_2}\frac{\kappa}{U_1^2}\frac{\Delta p}{p} = \frac{3s}{s-1}\frac{\kappa}{U_1^2}\frac{\Delta p}{p}$$

U and K_{xx} change discontinuously across the shock (Giacalone)

$$\tau_{acc} = p\frac{\Delta p}{p} = \frac{3s(t)}{s(t)-1}\frac{\kappa(t,p,r)}{U_1^2}$$

Maximum particle energy

- The maximum particle energy can be determined by equating the dynamic timescale of the shock with the acceleration timescale (Drury, 1983; Zank et al., 2000).

$$R(t) \Big/ \left(dR/dt\right) = \frac{3s}{s-1} \int_{p_{inj}}^{p_{\max}} \frac{\kappa\left(t, p', r\right)}{U_1^2} d\left(\ln p'\right)$$

Diffusion coefficient at parallel shock

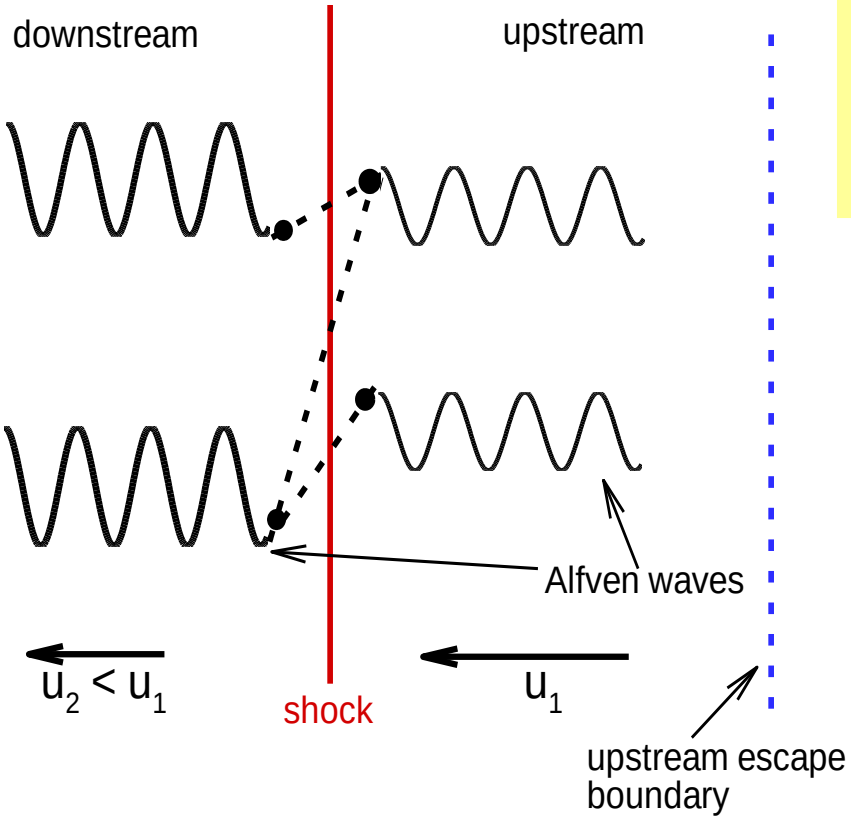

Near the shock front, Alfven waves are responsible for particle scattering. The particle distribution f, and wave energy density A are coupled together through:

$$\frac{\partial A}{\partial t} + u\frac{\partial A}{\partial r} = \Gamma A - \gamma A,$$

$$\frac{\partial f}{\partial t} + u\frac{\partial f}{\partial r} - \frac{p}{3}\frac{\partial u}{\partial r}\frac{\partial f}{\partial p} = \frac{\partial}{\partial r}\left(\kappa\frac{\partial f}{\partial r}\right),$$

$$\kappa(p) = \frac{\kappa_0}{A(k)}\frac{B_0}{B}\frac{(p/p_0)^2}{\sqrt{(m_p c/p_0)^2 + (p/p_0)^2}},$$

$$\kappa_0 = \frac{4}{3\pi} r_{g0} c = \frac{4}{3\pi}\frac{p_0 c}{eB_0},$$

Gordon et al., 1999 used to evaluate wave intensity. P_max, N_inj, p_inj, s, etc. Bohm limited applied when wave energy density per log bandwidth exceeds local solar wind magnetic energy density.

Maximum particle energy at quasi-parallel shock:

$$\frac{R(t)}{\dot{R}(t)} \gg \frac{q(t)}{u_1^2}\int_{p_{inj}}^{p_{\max}} k(p)\,d(\ln(p)) = \frac{q(t)}{\dot{R}^2(t)}\left(\frac{5M^2(t)+3}{M^2(t)+3}\right)\int_{p_{inj}}^{p_{\max}} k(p)\,d(\ln(p))$$

Age Strength Magnetic field heliocentric dependence

$$p_{\max} = \left\{\frac{5M^2(t)+3}{M^2(t)+3}\frac{R(t)\dot{R}(t)}{q(t)k_0}\frac{B}{B_0} + \sqrt{\left(\frac{m_p c}{p_0}\right)^2 + \left(\frac{p_{inj}}{p_0}\right)^2} - \frac{m_p c}{p_0}\right\}^{1/2}$$

$$\frac{B}{B_0} = \left(\frac{R_0}{r}\right)^2\left[1+\left(\frac{\Omega_0 R_0}{u}\right)^2\left(\frac{r}{R_0}-1\right)^2\sin^2 q\right]^{1/2}$$

Maximum energies for protons

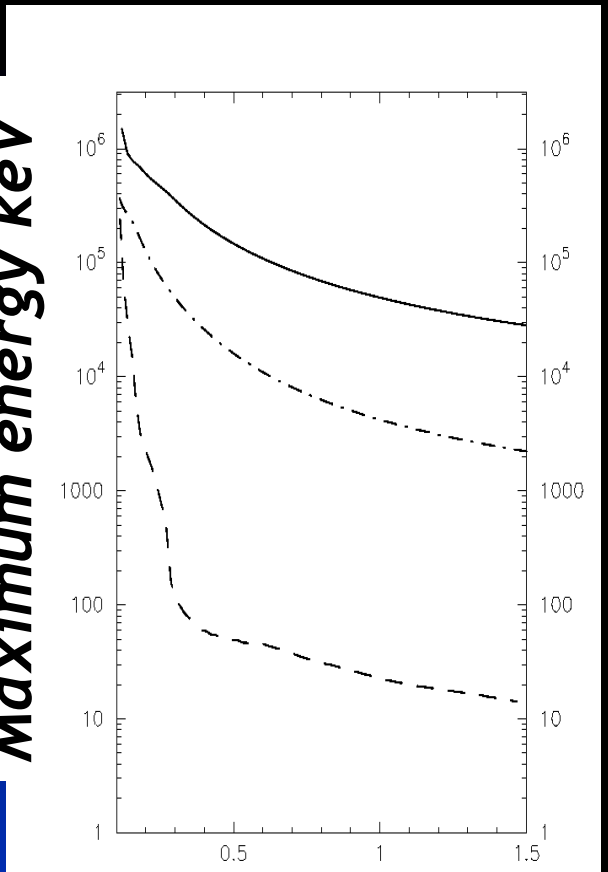

Strong, medium, weak shock examples

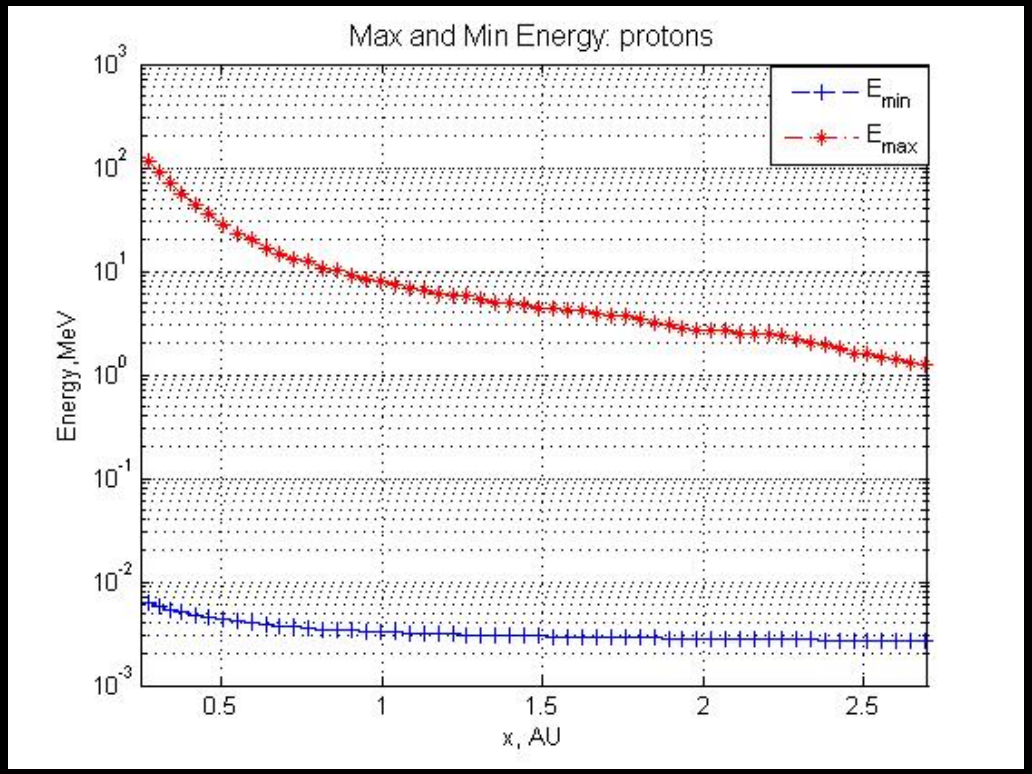

SEP Event # 215 (shock arrival at ACE: Sept. 29, 2001, 09:06 UT)

The maximum particle momentum obtained for a strong shock at early times can be as high as a few GeV – consistent with observations by Kahler [1994].

- What happens to the turbulence excited by the streaming protons?
- For quasi-|| shocks, turbulence excited by usual streaming instability; amplified on shock transmission
- Shell picture nice for describing the evolution of turbulence in downstream region – simplest is to assume WKB description as shell is convected outward and expands or to include turbulent dissipation.

Need to solve at the shock: $$\frac{\partial f}{\partial t}+u\frac{\partial f}{\partial r}-\nabla\cdot u\frac{p}{3}\frac{\partial f}{\partial p}=\frac{\partial}{\partial r}\left(\kappa_{rr}\frac{\partial f}{\partial r}\right)+Q$$

Local shock accelerated distribution:

Local maximum energy

$$f\left(t_k;t_k,p\right)=\frac{Q\left(t_k\right)\hbar R^2\left(t_k\right)}{p_0^3}\frac{3-q\left(t_k\right)}{\left[\left(p_{\max}\left(t_k\right)/p_{inj}\left(t_k\right)\right)^{3-q\left(t_k\right)}-1\right]}\left(\frac{p_0}{p_{inj}\left(t_k\right)}\right)^{3-q\left(t_k\right)}\left(\frac{p}{p_0}\right)^{-q\left(t_k\right)}\times\left\{H\left(p-p_{inj}\left(t_k\right)\right)-H\left(p-p_{\max}\left(t_k\right)\right)\right\}$$

Injection rate per unit area

Area of shock wave

Injection momentum

$$q\left(t_i\right)=3r_i/\left(r_i-1\right)$$

Particle Transport

Particle transport obeys Boltzmann(Vlasov) equation:

$$\frac{df(x,p,t)}{dt} + q[E + \mathbf{v} \times B] \bullet \frac{\partial f(x,p,t)}{\partial p} = \left.\frac{df(x,p,t)}{dt}\right|_{coll}$$

The LHS contains the material derivative and the RHS describes various "collision" processes.

- Collision in this context is pitch angle scattering caused by the irregularities of IMF and in quasi-linear theory

$$\frac{df}{dt} = \frac{\partial}{\partial \mu}\left(D_{\mu\mu}\frac{\partial f}{\partial \mu}\right)$$

- The result of the parallel mean free path $\lambda_{//}$, from a simple QLT is off by an order of magnitude from that inferred from observations, leading to a 2-D slab model.

$$\frac{\lambda}{10^6\,\mathrm{km}} = 8.30\,\frac{(B/B_0)^2}{\delta B_x^2/\delta B_{x0}^2}\left(\frac{l}{l_0}\right)^{2/3}\left(\frac{p/M_n}{B/B_0}\right)^{1/3}$$

Allows a Monte-Carlo technique.

CSPAR-UAH

Wave spectra and diffusion coefficient at shock

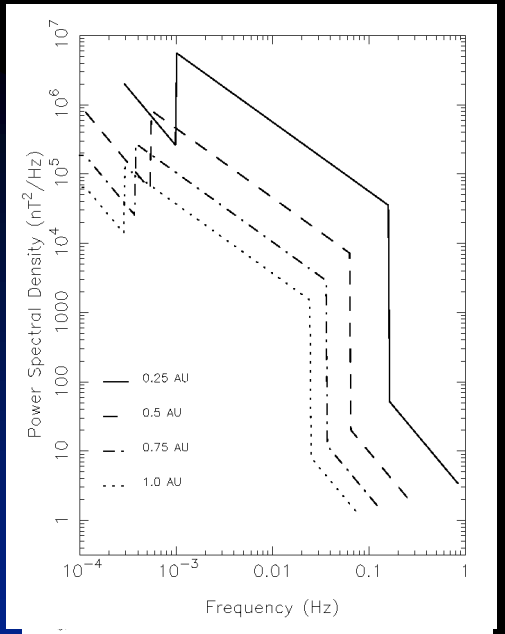

Wave intensity

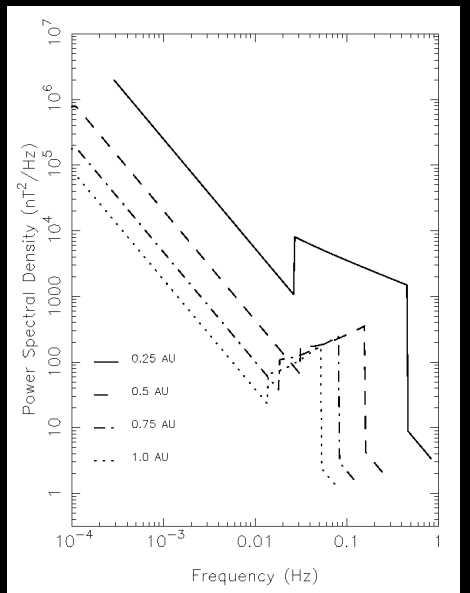

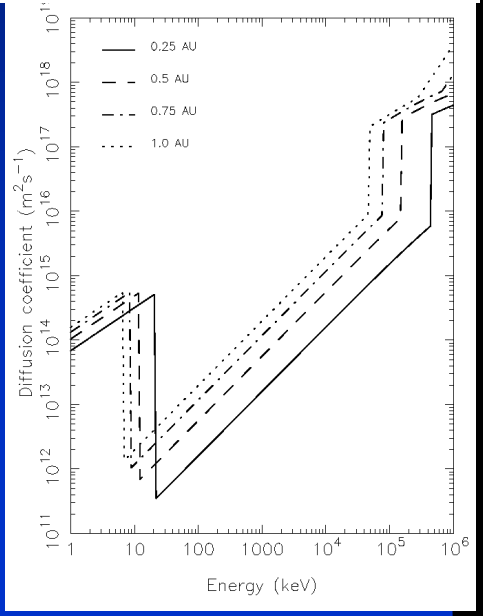

Diffusion coefficient

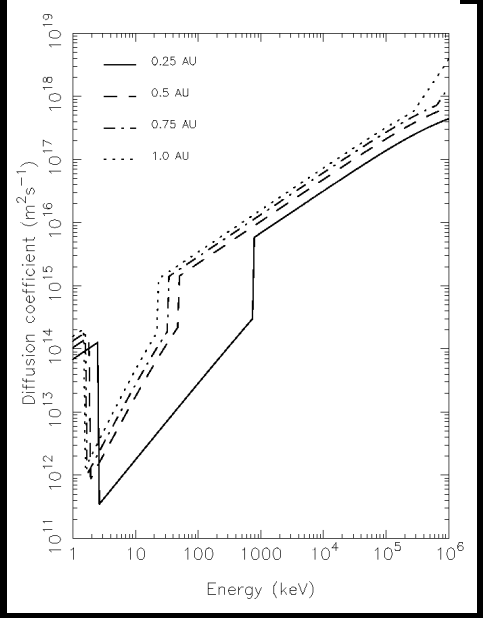

Strong shock

Weak shock

HEAVY IONS (CNO and Fe)

CNO: Q = 6, A = 14
Fe: Q = 16, A = 54

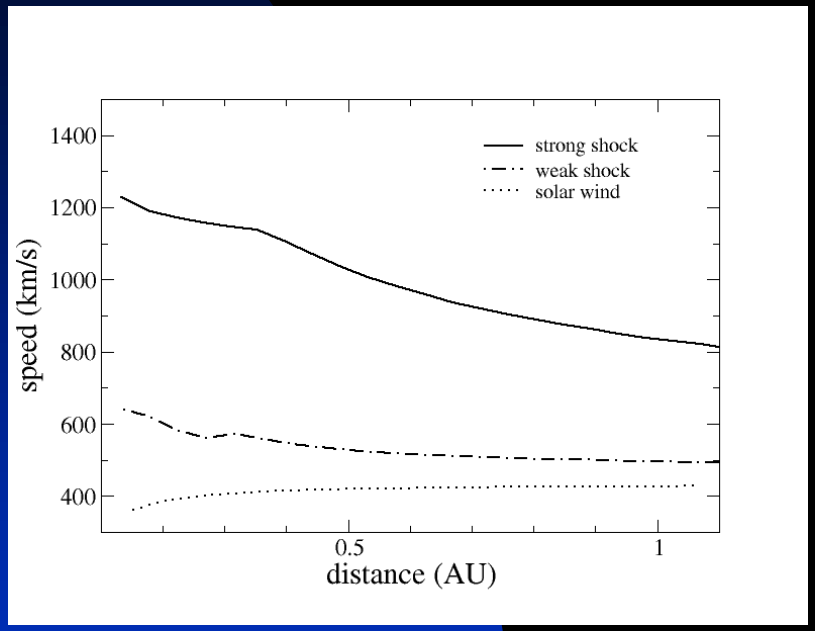

Shock speeds for strong and a weak shock.

Effect of heavy ions is manifested through the resonance condition, which then determines maximum energies for different mass ions and it determines particle transport - both factors that distinguish heavy ion acceleration and transport from the proton counterpart.

$$k = \frac{\gamma m_p \Omega}{m p}$$

$$\Omega = \frac{(Q/A)eB}{\gamma m_p c}$$

$$\lambda_{\perp} = \lambda_0 \left(\frac{\tilde{p}c}{1GeV}\right)^{1/3} \left(\frac{A}{Q}\right)^{1/3} \left(\frac{r}{1AU}\right)^{2/3}$$

Maximum accelerated particle energy

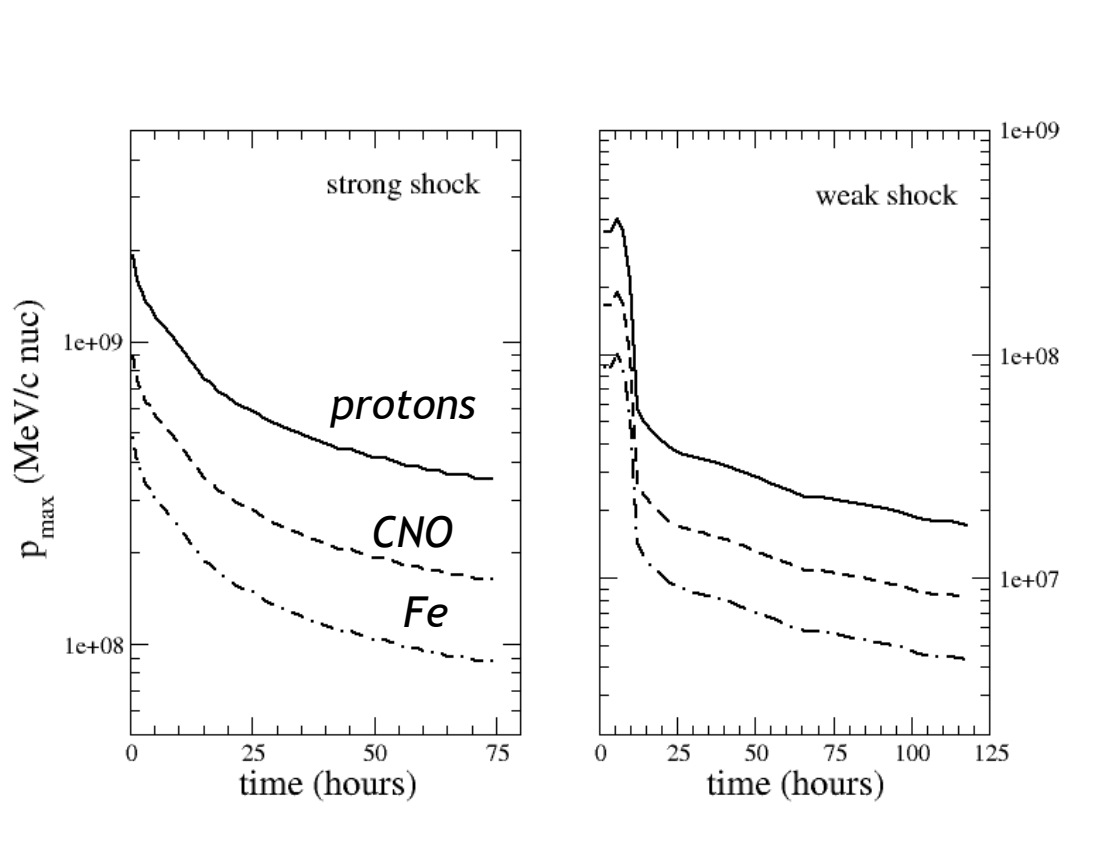

The maximum energy accelerated at the shock front. Particles having higher energies, which are accelerated at earlier times but previously trapped in the shock complex, will "see" a sudden change of κ. The maximum energy/nucleon for CNO is higher than iron since the former has a larger Q/A, thus a smaller κ.

Bohm approximation used throughout strong shock simulation but only initially in weak shock case.

WHAT ABOUT WAVE EXCITATION UPSTREAM?

Quasi-linear theory (Lee, 1983; Gordon et al, 1999): wave excitation proportional to cos ψ i.e.,

$$\frac{\partial I}{\partial t} \approx 0$$

at a highly perpendicular shock.

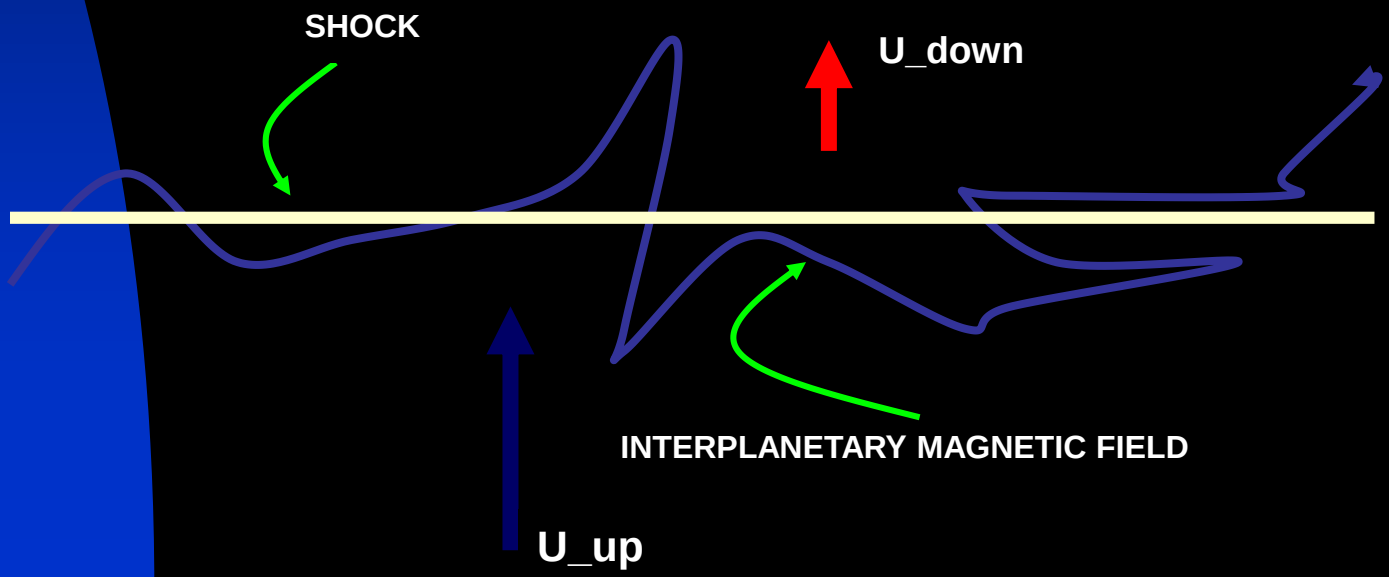

INTEGRAL FORM OF THE NONLINEAR GUIDING CENTER THEORY

Matthaeus, Qin, Bieber, Zank [2003] derived a nonlinear theory for the perpendicular diffusion coefficient, which corresponds to a solution of the integral equation

$$\kappa_{xx} = \frac{a^2 v^2}{3B_0^2} \int_0^\infty \frac{S_{xx}(\mathbf{k})\, d^3\mathbf{k}}{v/\lambda_{\parallel} + k_\perp^2 \kappa_{xx} + k_z^2 \kappa_{zz}}$$

Superposition model: 2D plus slab

$$S_{xx}(\mathbf{k}) = S_{xx}^{2D}\delta(k_\perp)\delta(k_z) + S_{xx}^{slab}\delta(k_\perp)$$

Solve the integral equation approximately (Zank, Li, Florinski, et al, 2004):

$$\lambda_{xx} \approx \left(\sqrt{3}\pi a^2 C\right)^{2/3} \left(\frac{\langle b_{2D}^2 \rangle}{B_0^2}\right)^{2/3} \lambda_{2D}^{2/3} \lambda_{\parallel}^{1/3} \left[1 + \frac{(a^2 C)^{1/3}}{(\sqrt{3}\pi)^{2/3}} \frac{\langle b_{slab}^2 \rangle}{\langle b_{2D}^2 \rangle^{2/3} (B_0^2)^{1/3}} \frac{\min(\lambda_{slab}, \lambda_{\parallel}/\sqrt{3})}{\lambda_{slab}^{2/3} \lambda_{\parallel}^{1/3}} \left(4.33 H(\lambda_{slab} - \lambda_{\parallel}/\sqrt{3}) + 3.091 H(\lambda_{\parallel}/\sqrt{3} - \lambda_{slab})\right)\right]^{2/3}$$

$\lambda_{\parallel}$ modeled according to QLT.

Maximum and injection energies

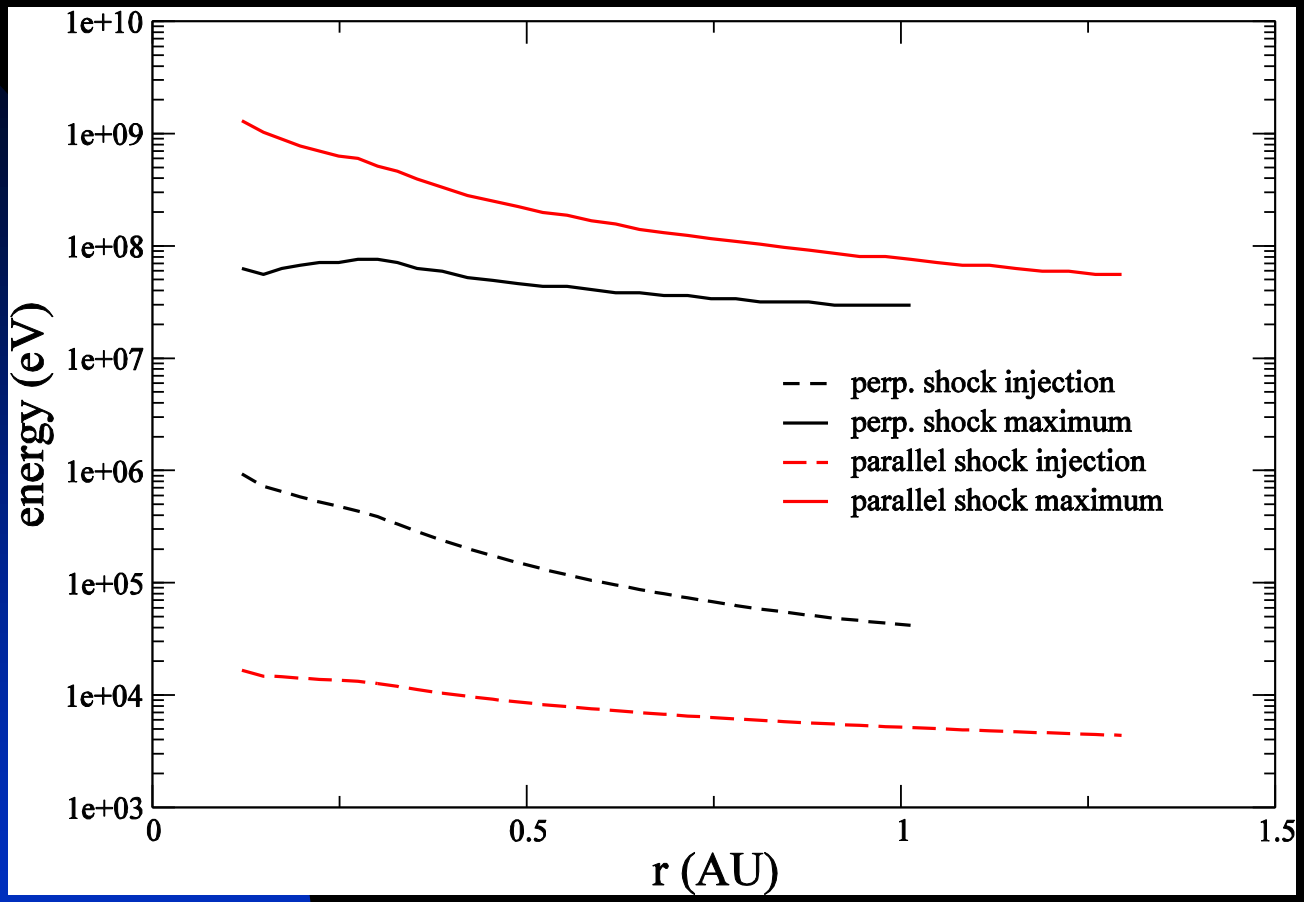

Remarks: 1) Parallel shock calculation assumes wave excitation implies maximum energies comparable

3) Injection energy at Q-perp shock much higher than at Q-par therefore expect signature difference in composition

Time evolution of number density in phase space

- Snap shots of the number density observed at 1 AU prior to the shock arrival at t = 1/20, 2/20, …. T, with a time interval of 1/20 T in (v_par, v_perp)-space.
- Coordinates:

$$Z_x = cos(\theta_{\hat{\mathbf{B}},\hat{\mathbf{p}}})(log(p/\mathrm{MeV}) - 4.25);$$
$$Z_y = sin(\theta_{\hat{\mathbf{B}},\hat{\mathbf{p}}})(log(p/\mathrm{MeV}) - 4.25).$$

- B field along positive Zx direction
- Particle energies from innermost to outermost circle are K = 4.88, 8.12, 10.47, 15.35, 21.06, 30.75, 50.80, 100.13 MeV respectively.

The next figures exhibit the following characteristics:

- At early times, more high energy particles cross 1 AU along +B direction, followed by lower energies later.

- Number density of higher energy particles at later times exhibits a “reverse propagation” feature corresponding to A < 0.

- The gap at Θ = 90 degree reflects that particles must have a component along B to be observed.

CSPAR-UAH

Phase space evolution – time sequence

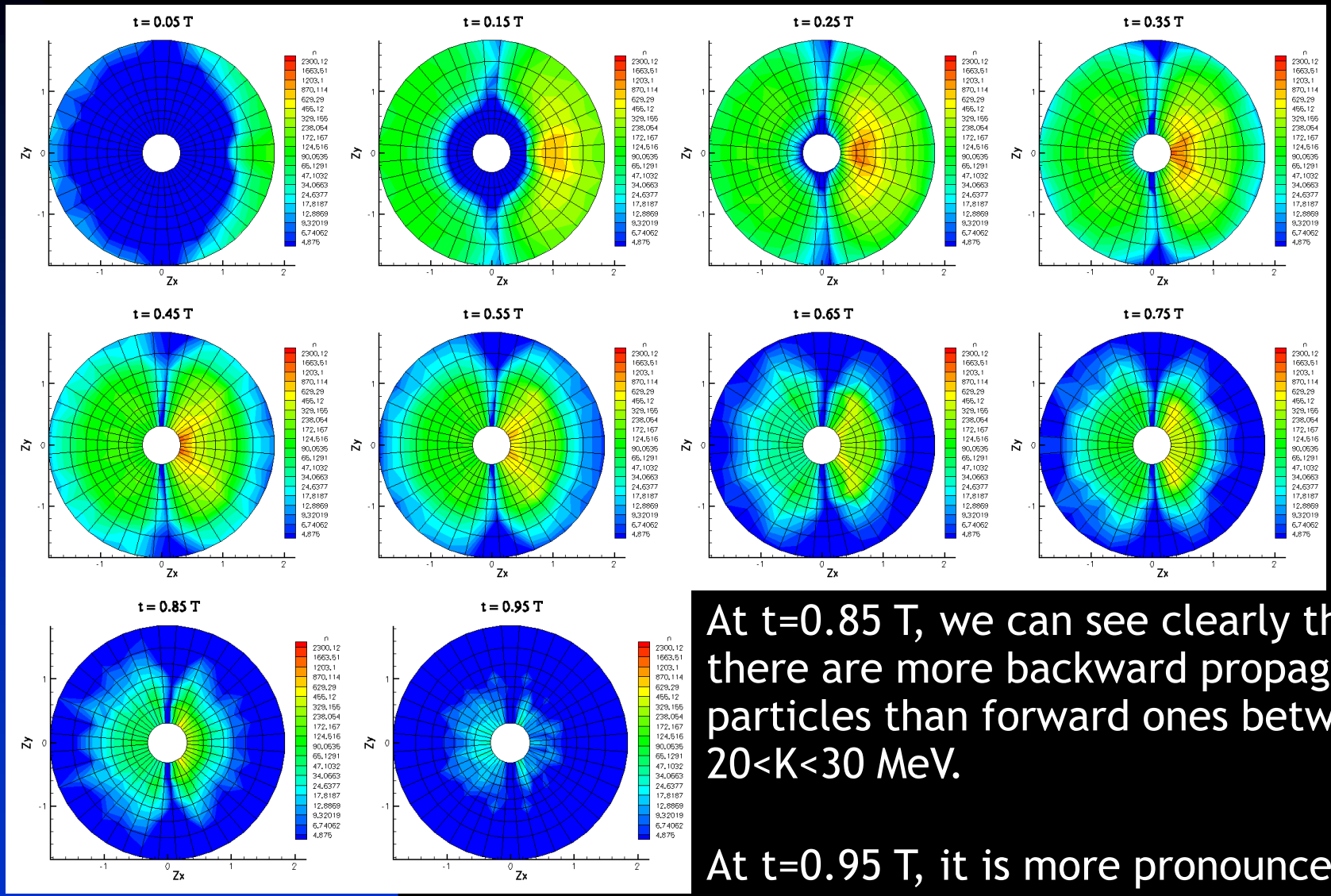

At t=0.85 T, we can see clearly that there are more backward propagating particles than forward ones between 20<K<30 MeV.

At t=0.95 T, it is more pronounced for K~10 MeV.

Multiple particle crossings at 1AU

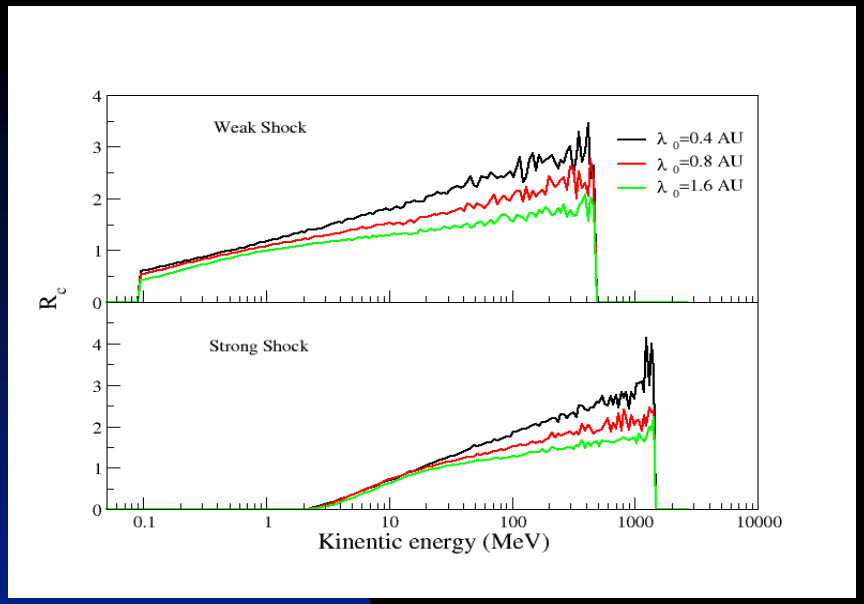

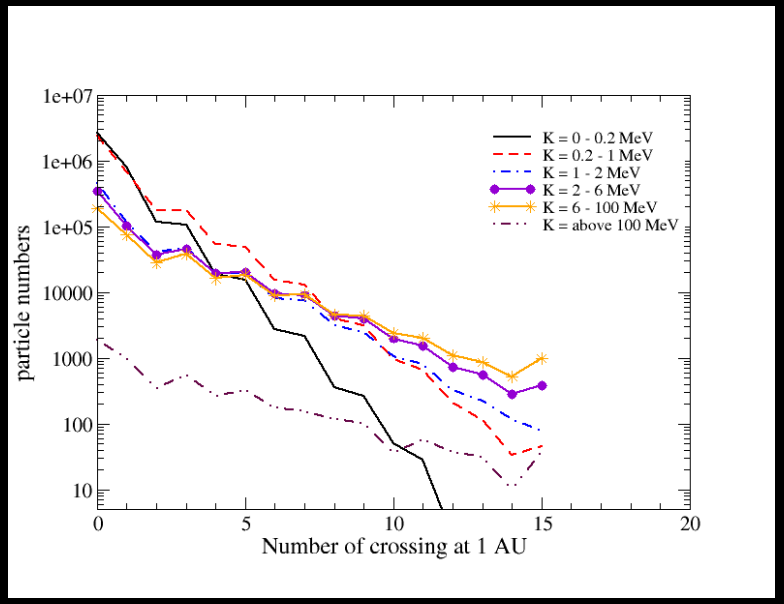

$$R_c(K) \equiv \frac{\text{number of particles of energy K that cross 1 AU}}{\text{number of particles of energy K that leave the shock}}$$

Due to pitch angle scattering, particles, especially of high energies, may cross 1 AU more than once, and thus from both sides. In an average sense, a 100 MeV particle has Rc ~ 2, or on average, two crossings. Histogram shows that some particles may cross as many as 15 times. A smaller mfp leads to a larger Rc since particles with smaller mfp will experience more pitch angle scatterings.

CSPAR-UAH

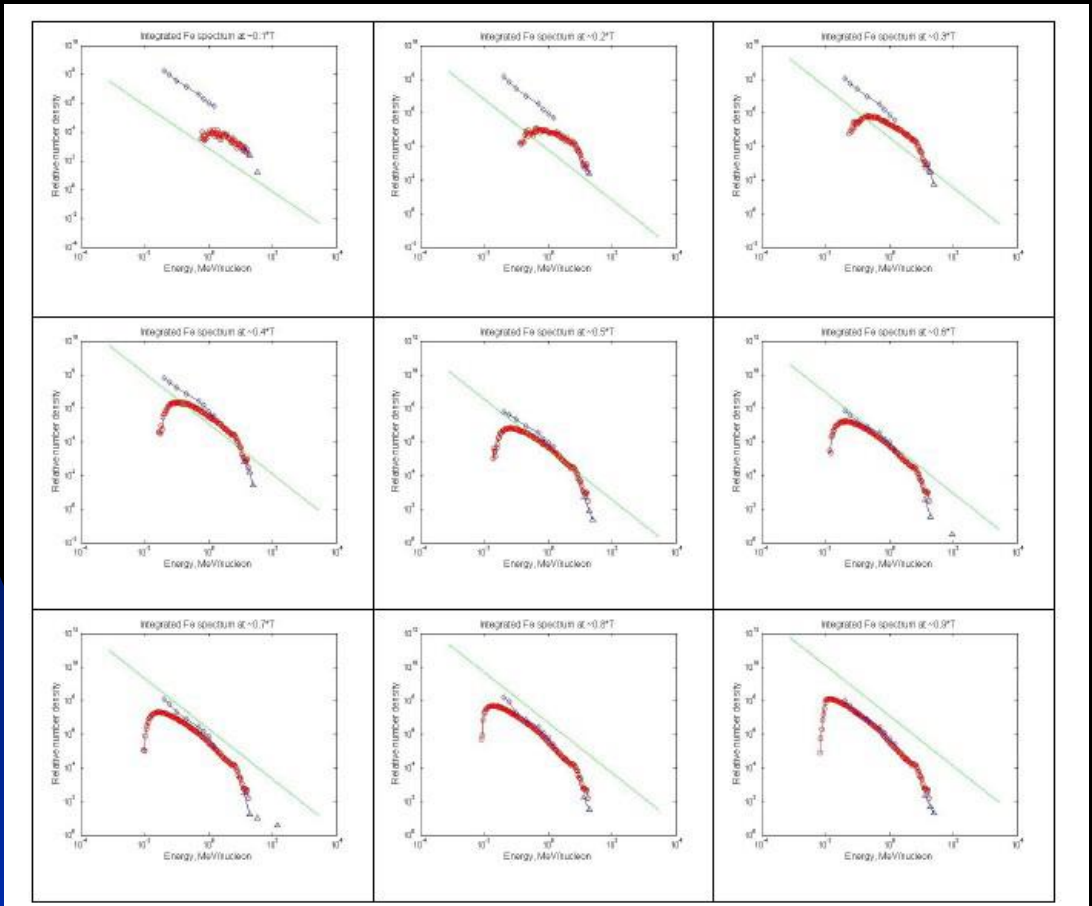

Dynamical spectra of iron ions averaged over consecutive ~5hrs time intervals until shock arrival at 1AU. ULEIS and SIS measurements are shown by blue diamonds and triangles, respectively. The straight line shows the theoretical limit for a power-law spectrum corresponding to shock parameters at 1 AU. Note the enhanced background at early times prior to the shock arrival at ~ 1AU.

SEP Event # 215 (shock arrival at ACE: Sept. 29, 2001, 09:06 UT)

Event integrated spectra

NOTE change in Fe/O ratio at about 10 MeV/nuc

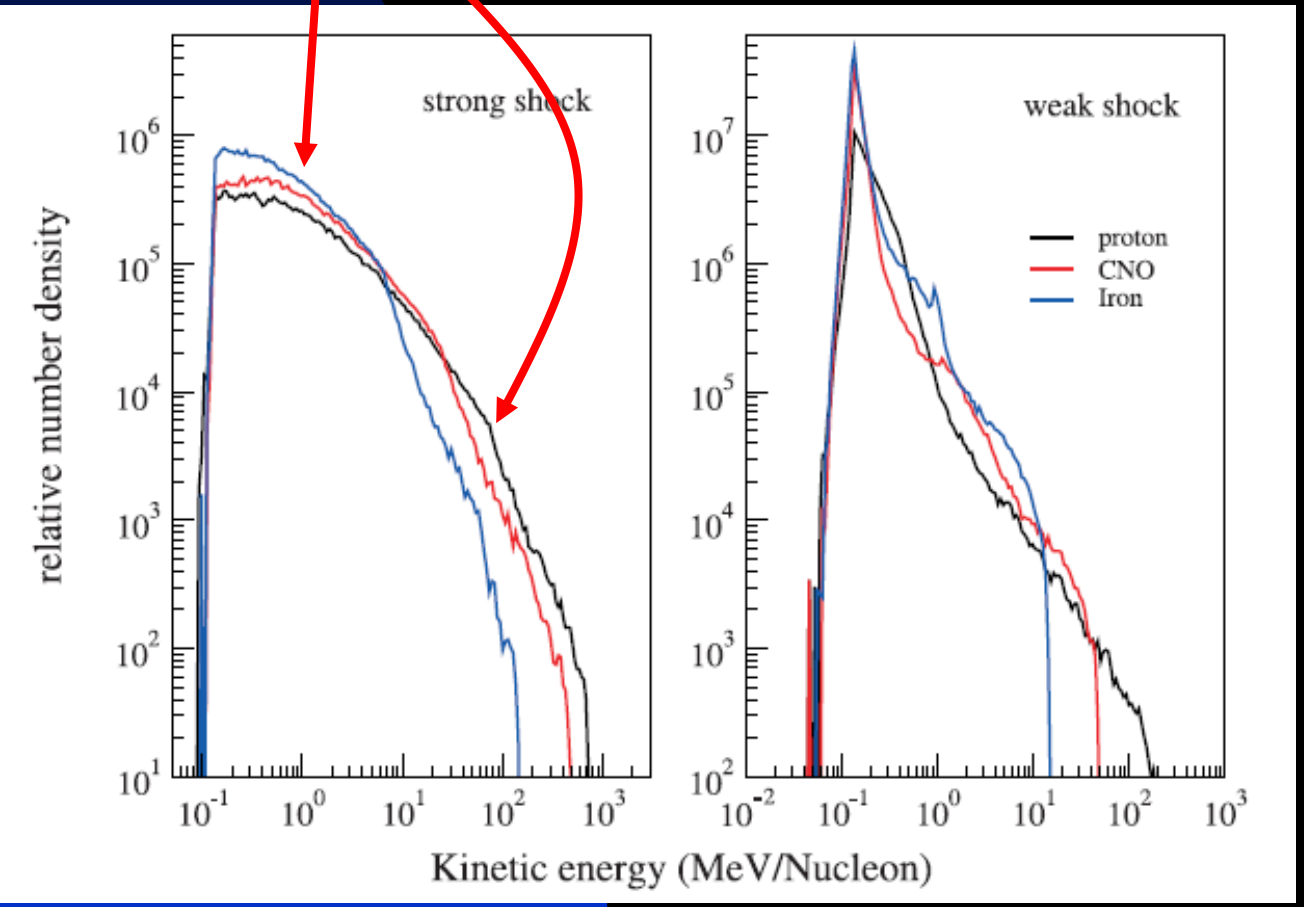

Iron Q = 14, A =56

CNO Q = 6. A = 14

Similar spectral indices at low energies, with Iron slightly softer.

Roll-over feature at high energy end with approximately $(Q/A)^2$ dependence.

Count only those particles before the shock arrival.

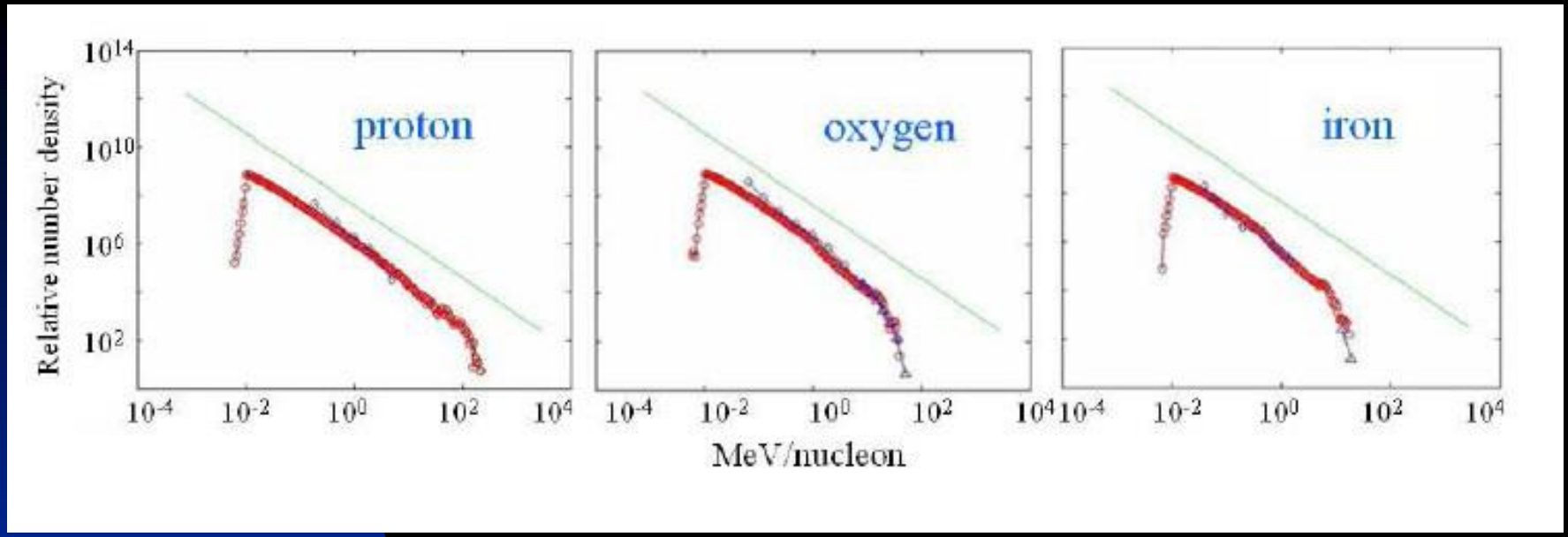

Event-integrated spectra for (a) protons, (b) oxygen and (c) iron ions. Modeling results are shown in red. ULEIS and SIS measurements integrated over the same time interval are shown by blue diamonds and triangles, respectively. The straight line shows the theoretical limit for a power-law spectrum corresponding to shock parameters at 1 AU. (Zank et al 2007; Verkhoglyadova et al. 2009).

SEP Event # 215 (shock arrival at ACE: Sept. 29, 2001, 09:06 UT)

Time intensity profiles

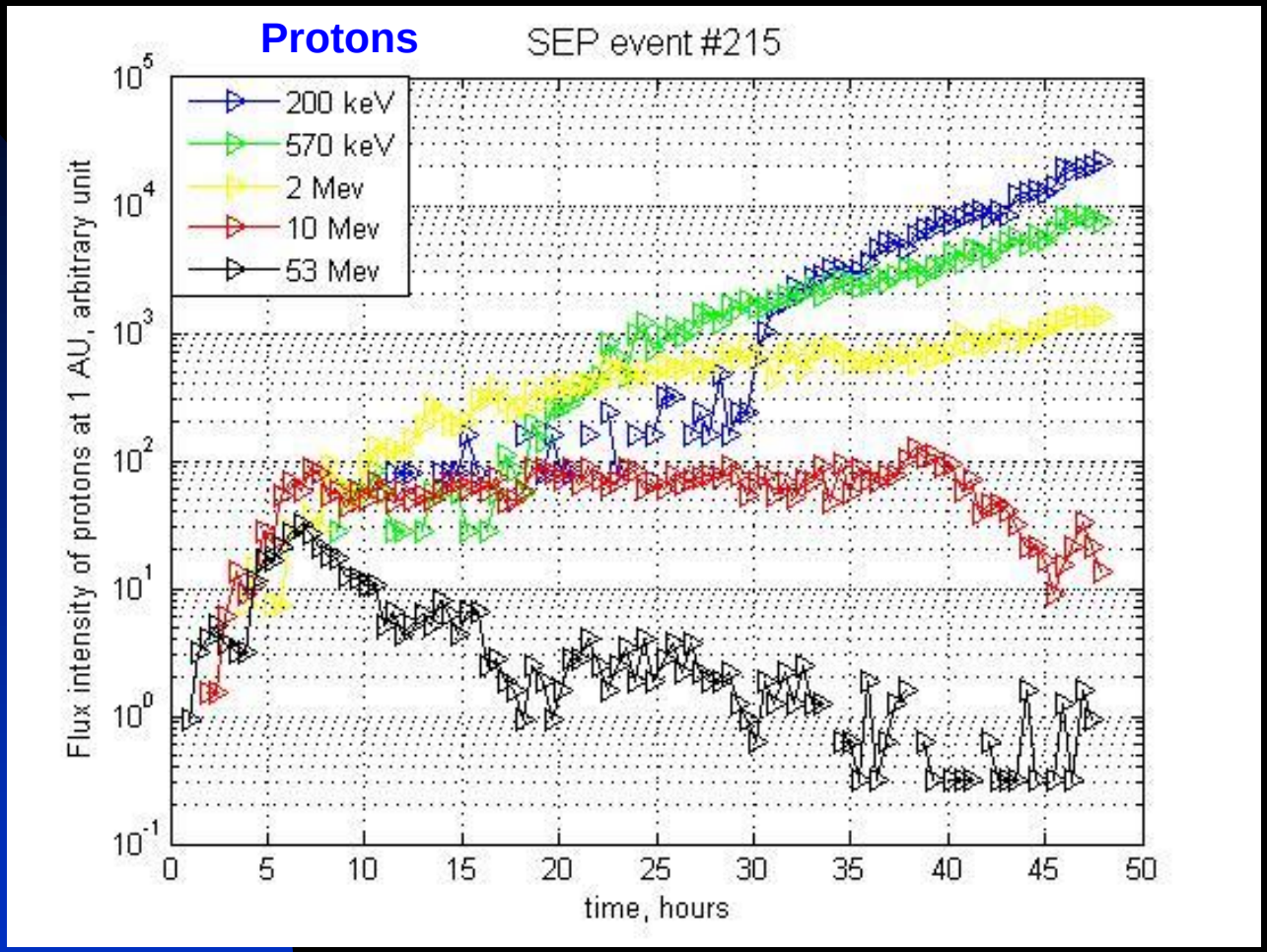

SEP Event # 215 (shock arrival at ACE: Sept. 29, 2001, 09:06 UT)

s=2.5

Time intensity profiles

Time intensity profiles of iron and oxygen ions. Representative energies are (from top to bottom): 0.2, 0.57, 2 and 10 MeV/nucleon. Time is in hours starting from the shock launch at 0.1 AU until the shock arrival at 1 AU

NOTE change in Fe/O ratio after 40 hours

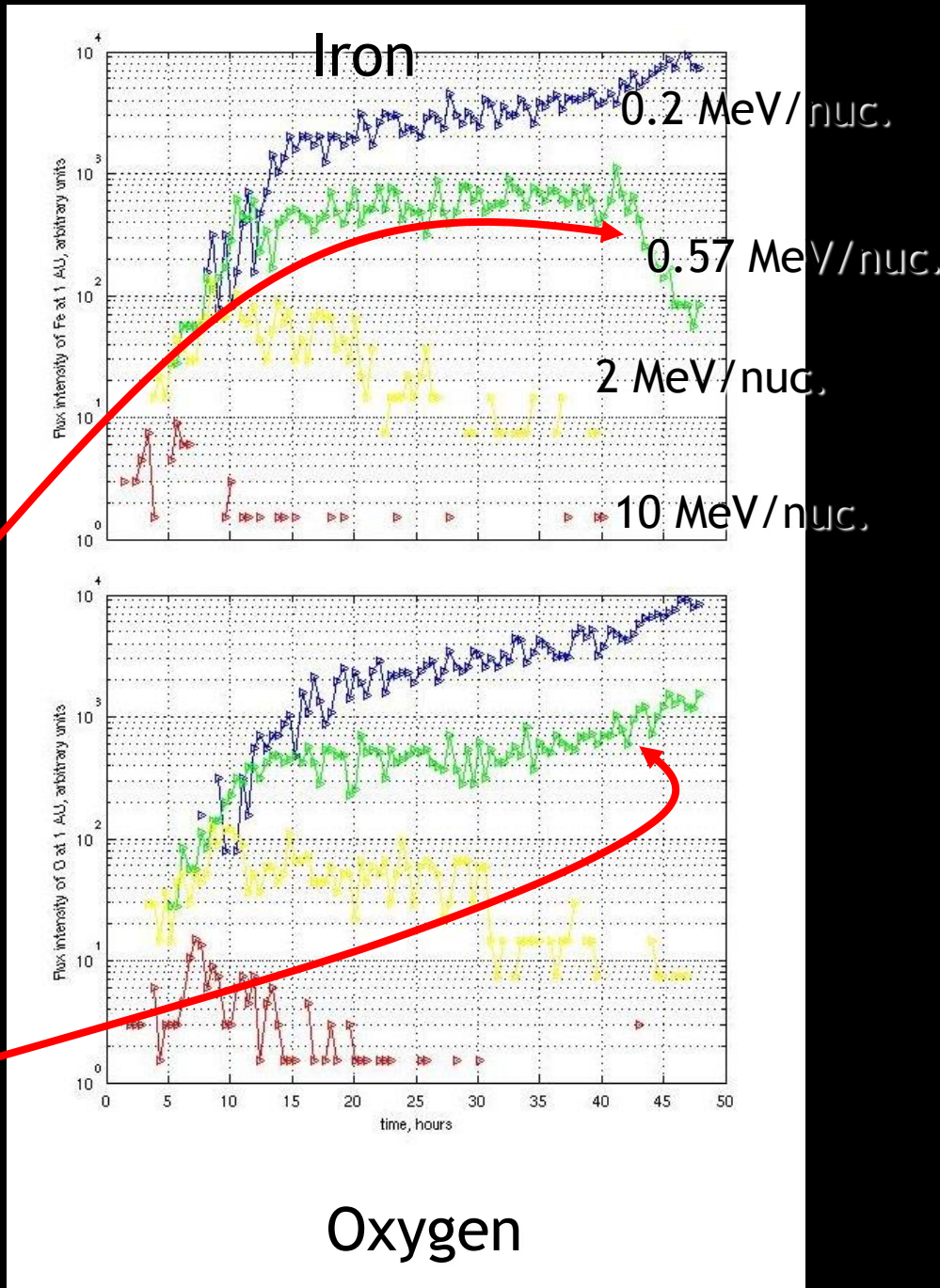

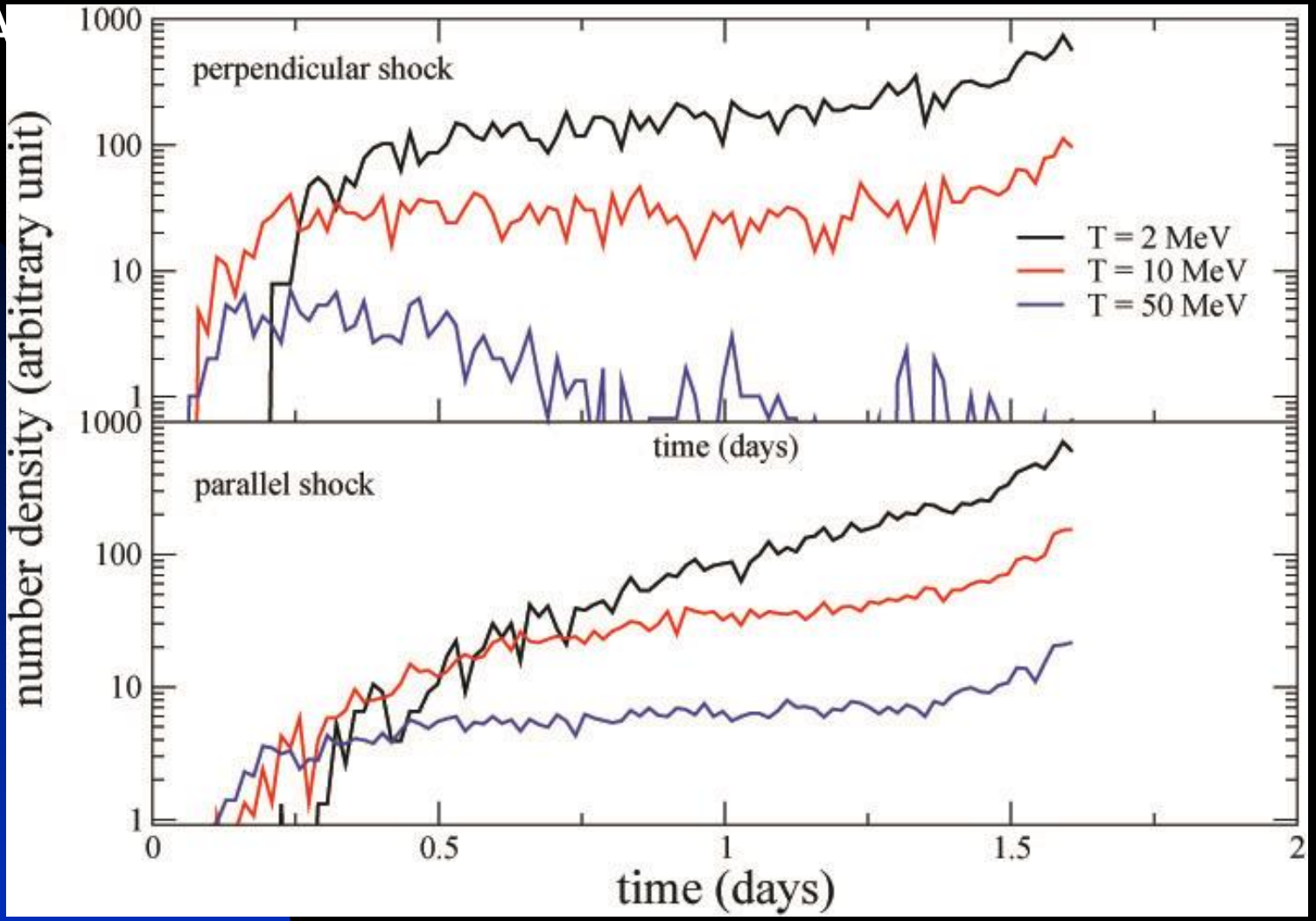

Intensity profiles emphasize important role of time dependent maximum energy to which protons are accelerated at a shock and the subsequent efficiency of trapping these particles in the vicinity of the shock. Compared to parallel shock case, particle intensity reaches plateau phase faster for a quasi-perpendicular shock – because K_perp at a highly perpendicular shock is larger than the stimulated K_par at a parallel shock, so particles (especially at low energies) find it easier to escape from the quasi-perpendicular shock than the parallel shock.

CSPAR-UAH

Modeling Particle Acceleration and Transport at a 2 2D CME-Driven Shock

Junxiang Hu, Gang Li, Xianzhi Ao, G.P. Zank, and O. Verkhoglyadova

submitted

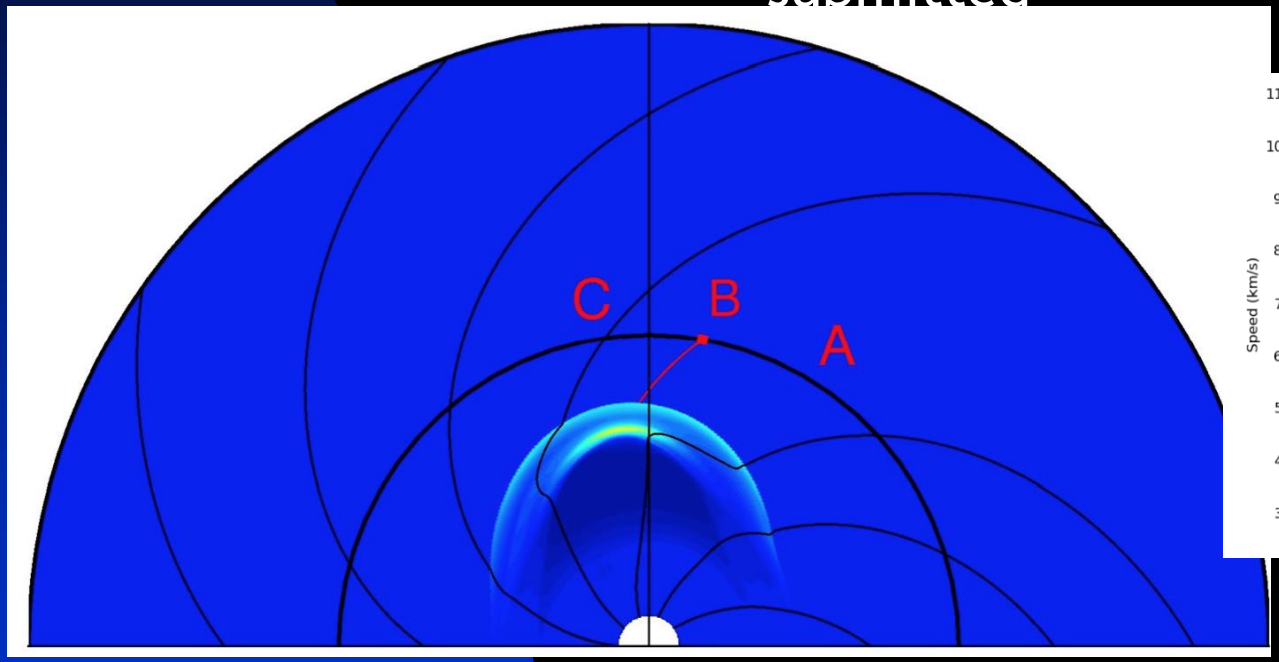

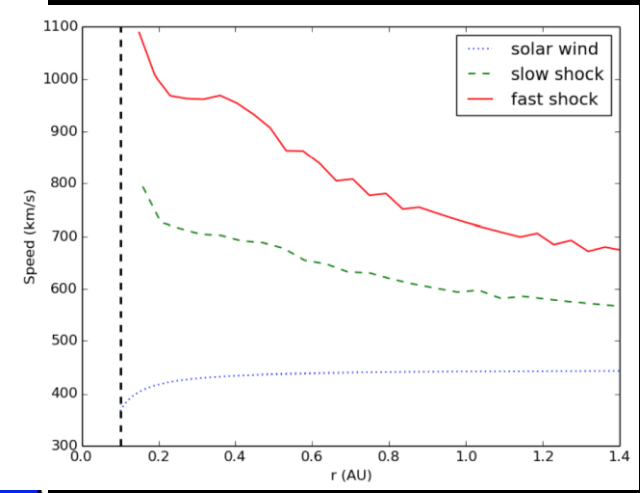

Fast CME-driven shock. Simulation domain 0.1 to 2 AU. The color scheme is the normalized density nr^2. The bold black semi-circle at 1 AU is Earth orbit. Three reference points A, B and C, at longitudes of 60°, 80° and 100°
Inset: Two shock radial speed examples at nose.

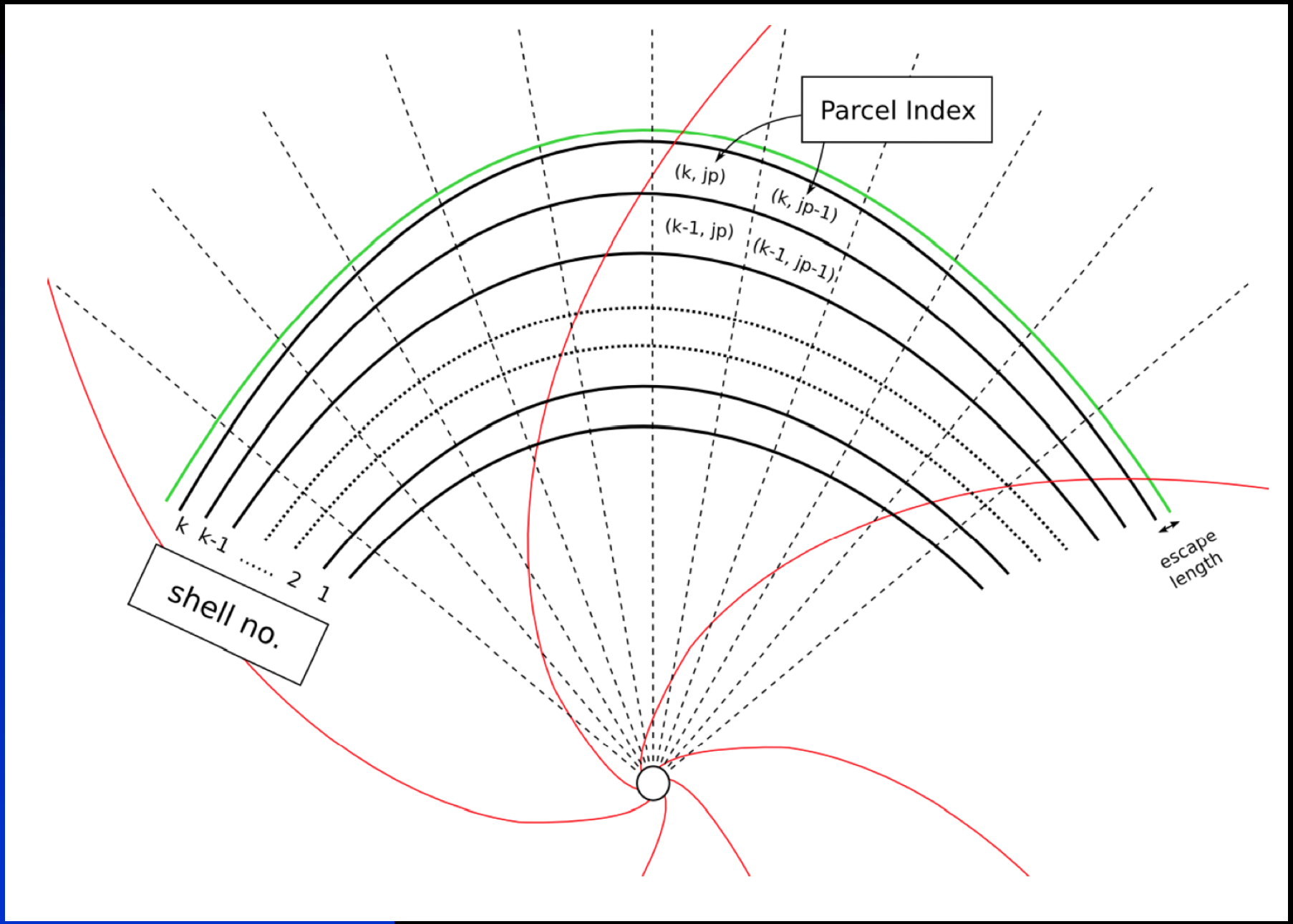
Parcel Index
(k, jp)
(k, jp-1)
(k-1, jp)
(k-1, jp-1)
k
k-1
.....
2
1
shell no.
escape
length

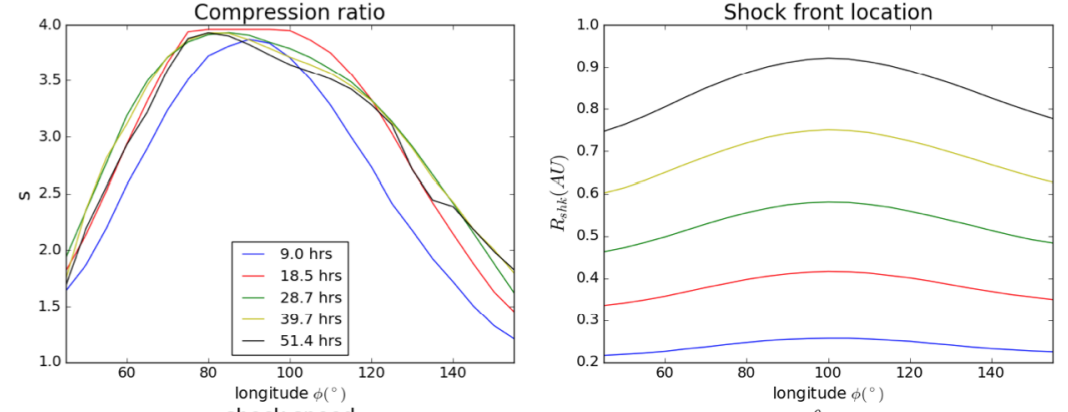

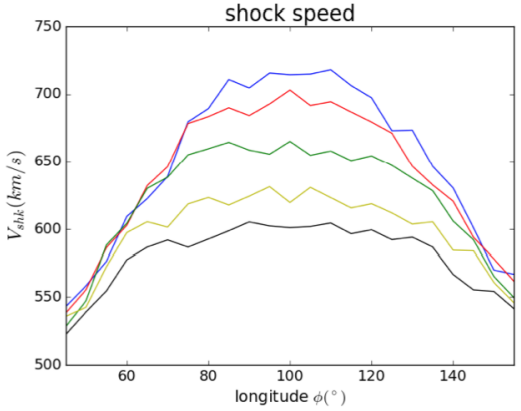

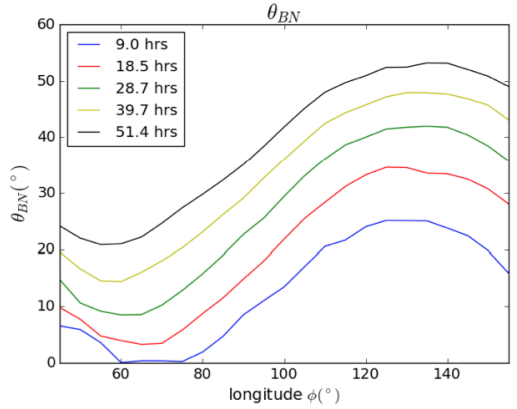

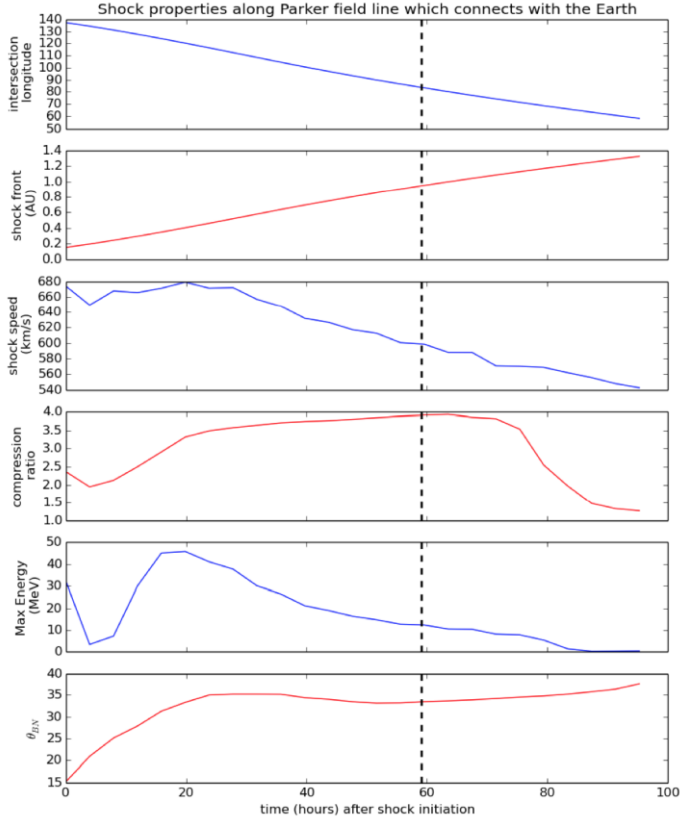

Slow shock (X2)

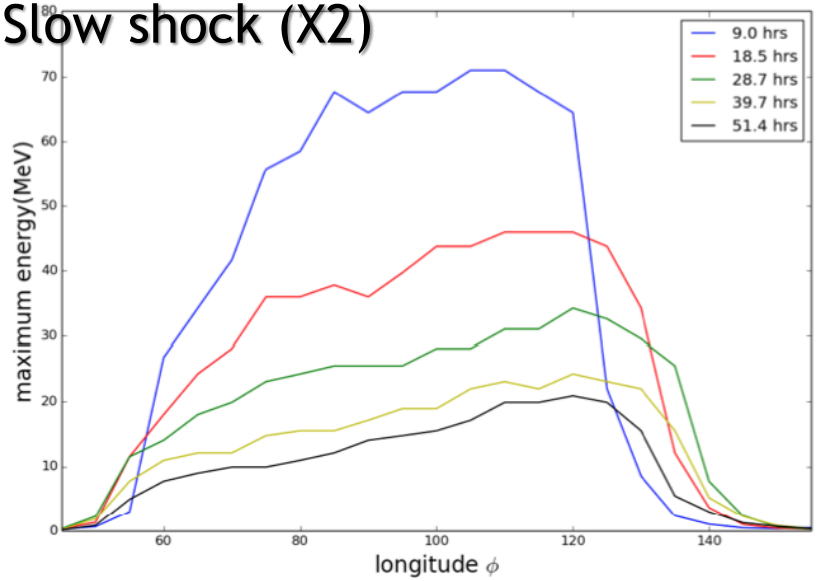

Fast shock (X3)

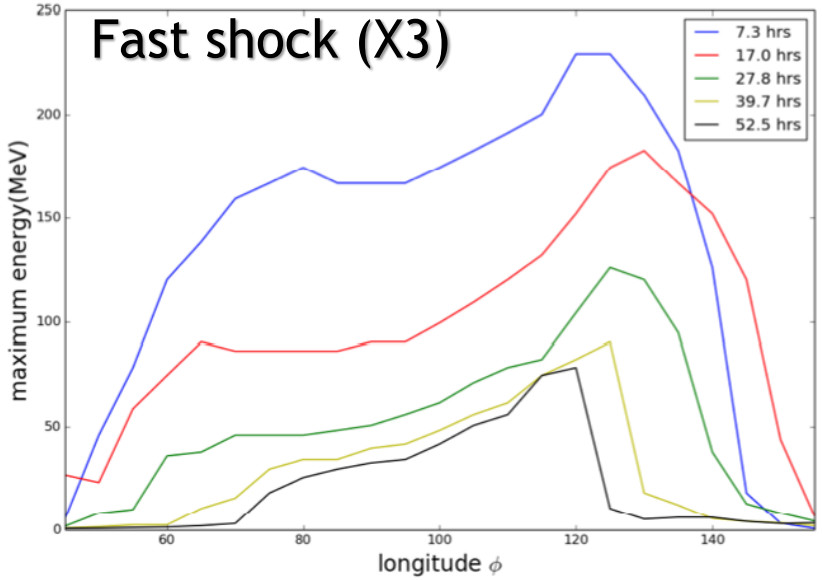

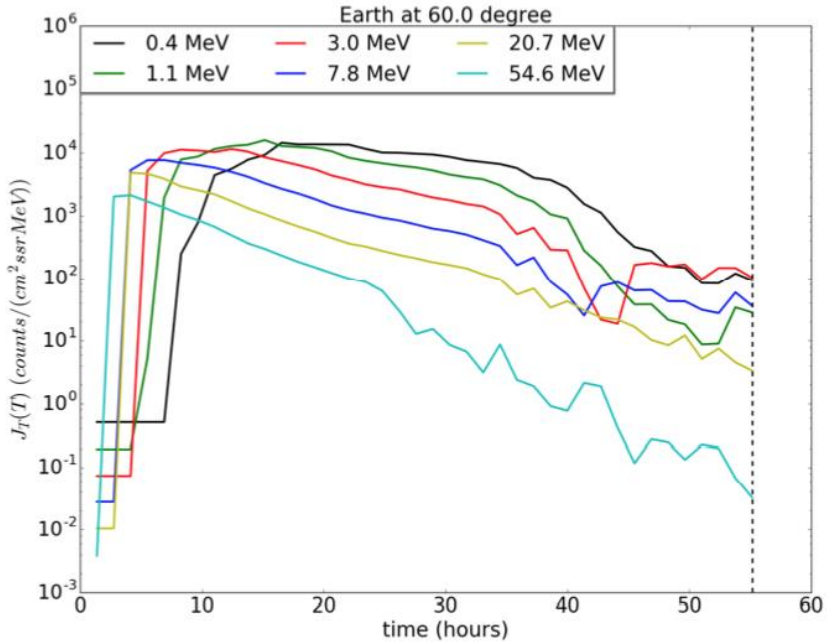

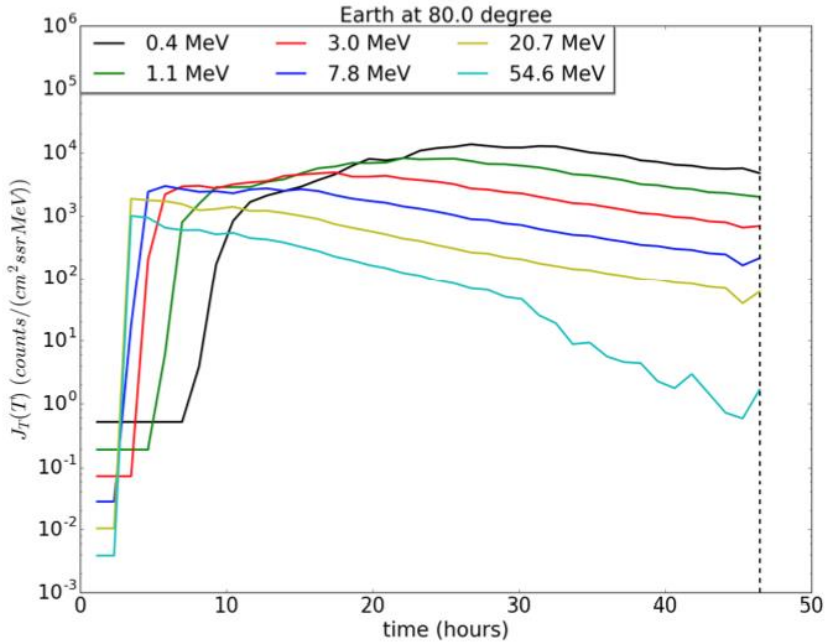

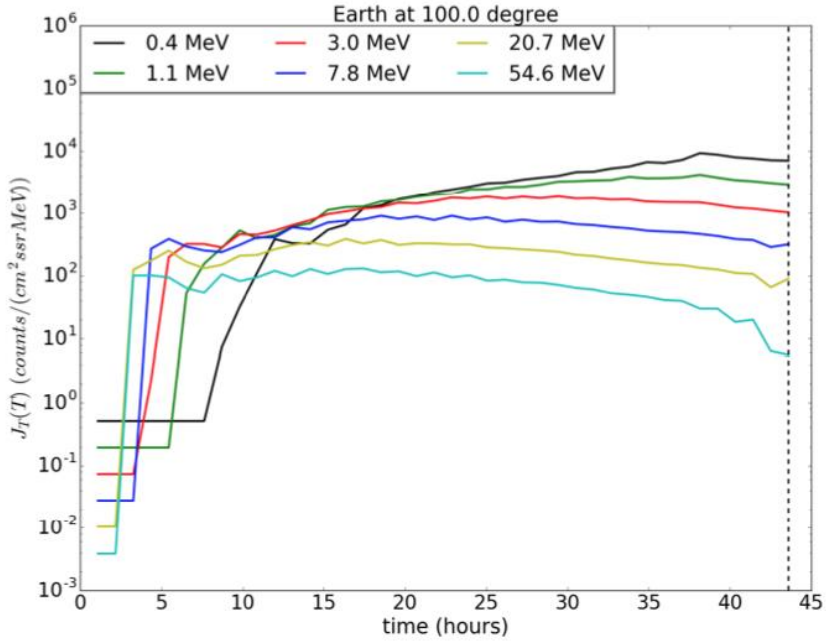

Time intensity profiles for protons at three different reference locations at 1 AU for the slow shock case.

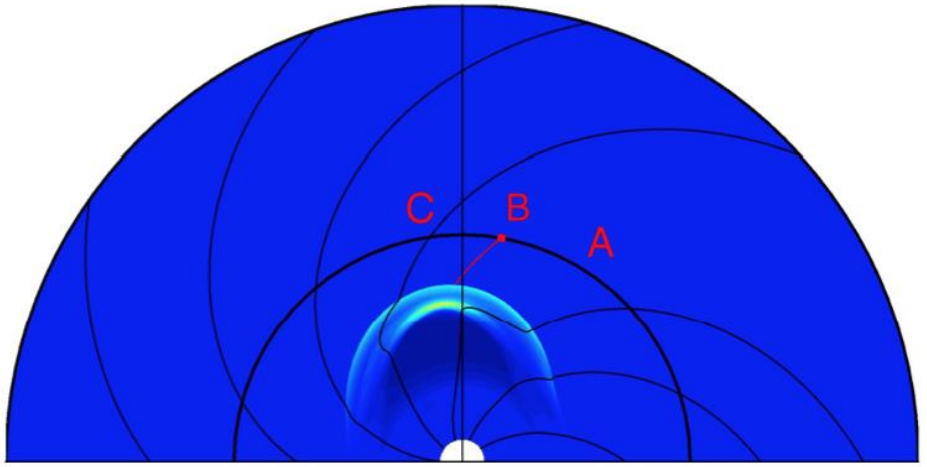

CSPAR-UAH

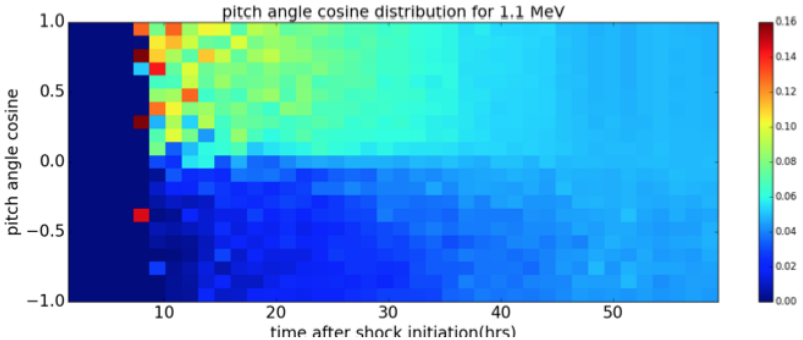

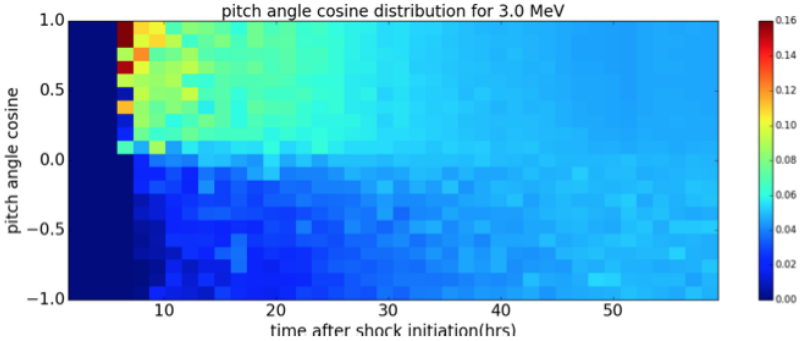

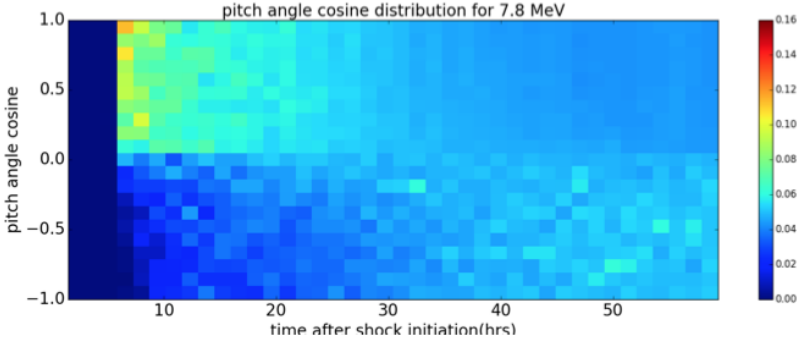

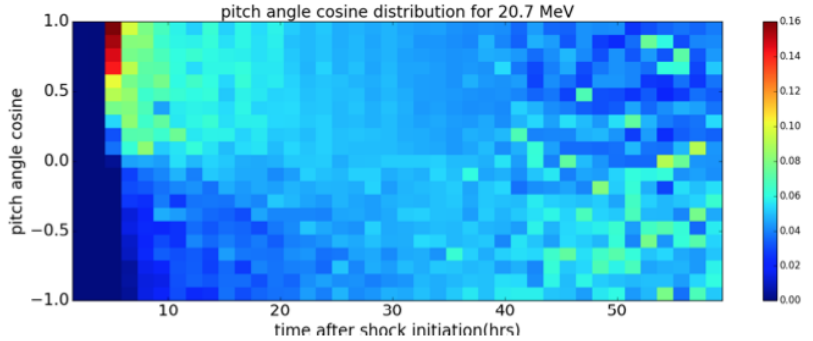

Pitch angle distributions at B ($\varphi = 80^{\circ}$) for four different energies

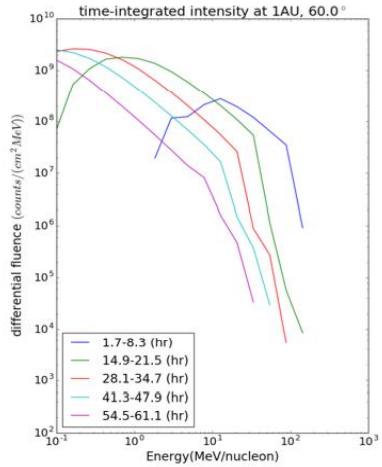

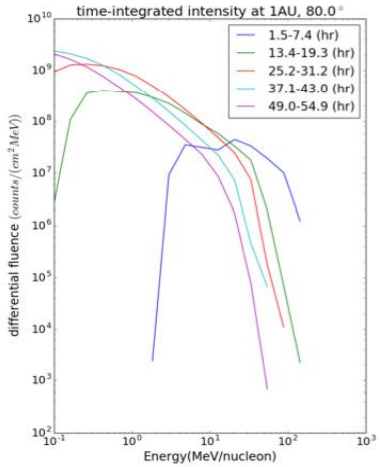

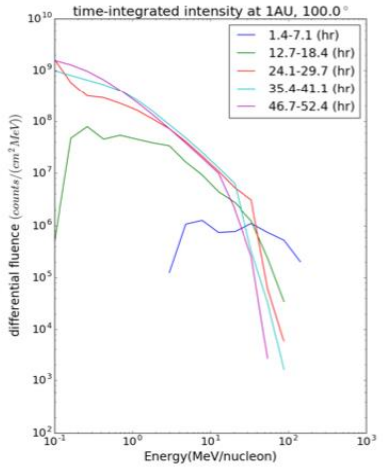

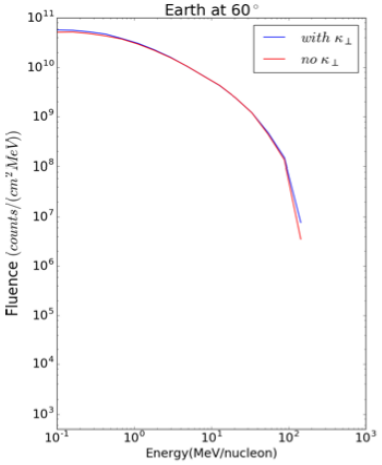

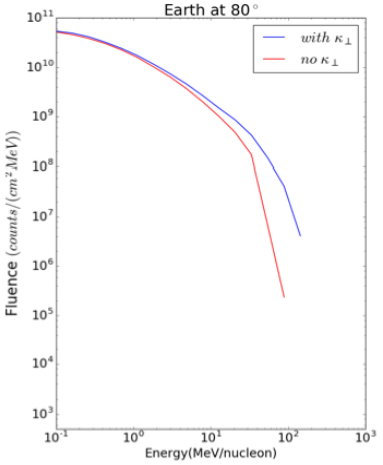

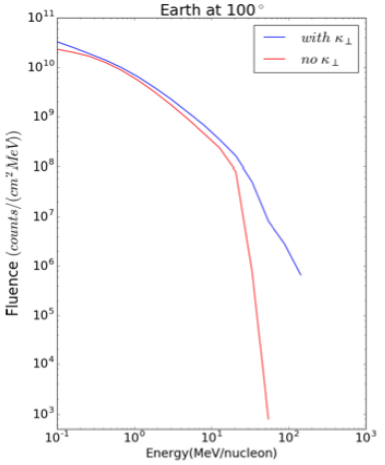

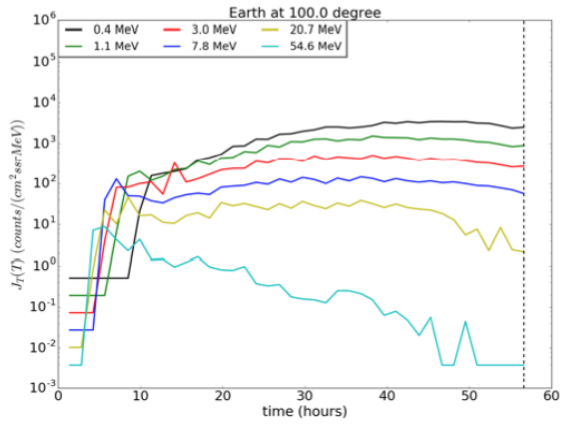

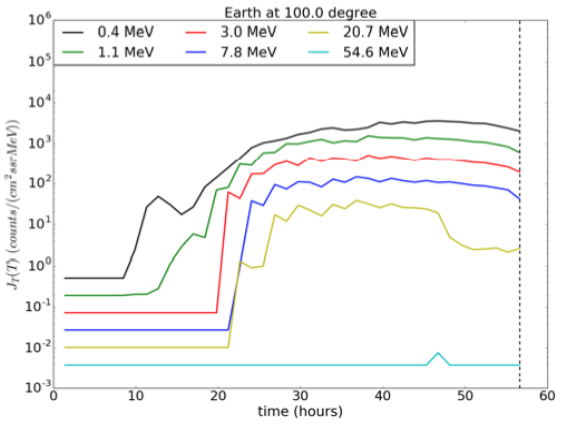

Time-integrated proton fluence at 1 AU. Left to right, point A ($\varphi = 60^\circ$), B (80°), and C (100°).

Event integrated proton fluence at 1AU. The red line shows results without $\kappa_\perp$ and blue with $\kappa_\perp$.

Time intensity profiles for 6 energies at C (100°). Left is for protons with $\kappa_\perp$ and right is for protons without $\kappa_\perp$.

CSPAR-UAH

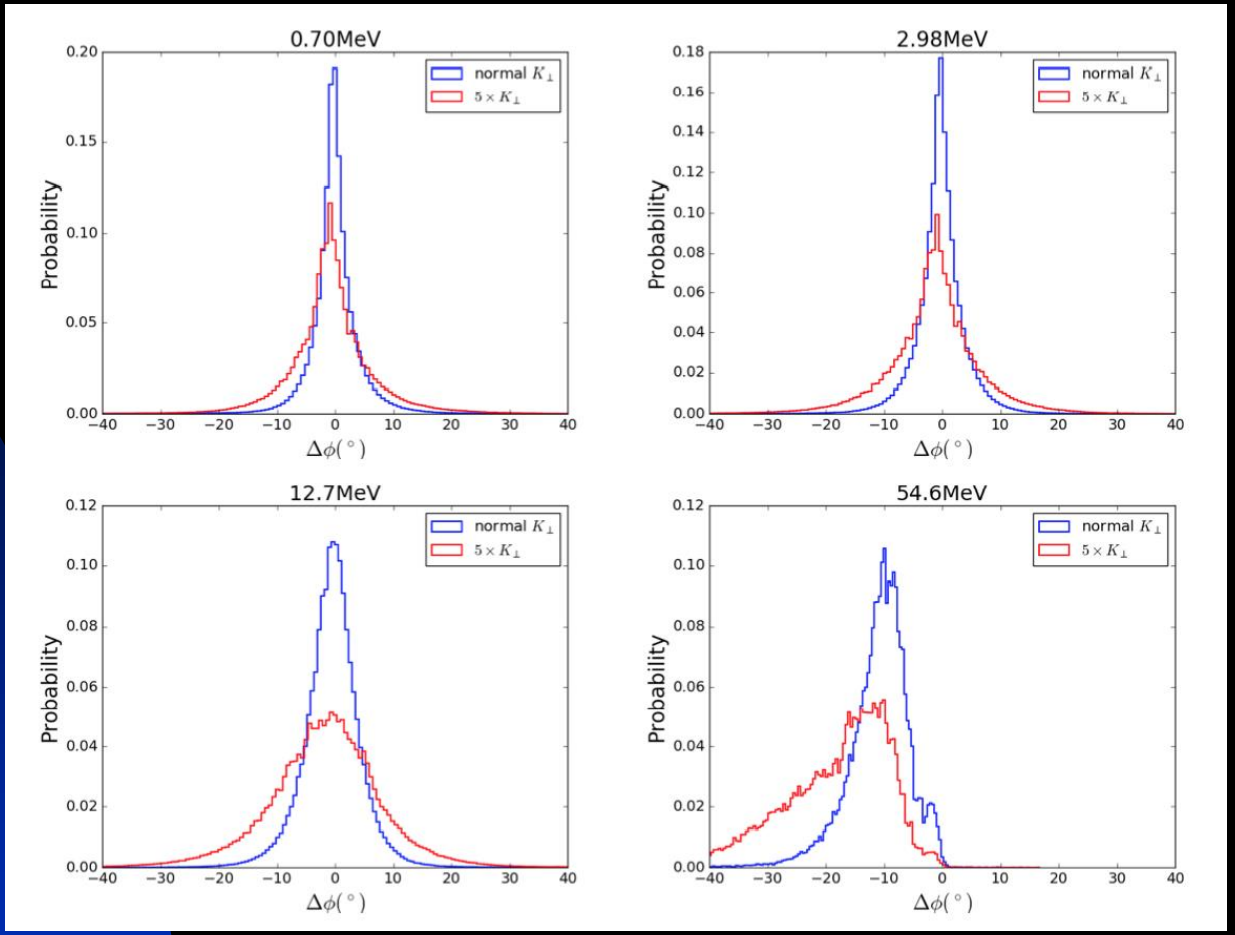

Longitudinal spreading Δφ of particles from its original field line on which it was accelerated at the shock. The histogram shows the angular separation between the two Parker field lines L_f and L_i, where L_f is the Parker field when the particle arrives 1 AU and L_i is the Parker field line when the particle leaves the shock. Blue lines use extended NLGC theory for $\kappa_\perp$ (Shalchi et al 2006. Red lines -- $\kappa_\perp$ increased by a factor of 5.

Conclusions:

- 1D PATH model can explain observations of many quasi-parallel events such as e.g., the large SEP event of Dec. 13, 2006.
- Based on the PATH model we can describe/understand main features of ion spectra and intensity profiles.
- Provides basis for developing and understanding 2D/3D iPATH model with perpendicular diffusion included.
- Different charge states for the particles and SW suprathermals will be included in iPATH model.